JOURNAL OF GEOPHYSICAL RESEARCH: EARTH SURFACE, VOL. 118, 519–541, doi:10.1002/jgrf.20032, 2013

New constraints on Greenland ice sheet dynamics during the last glacial cycle: Evidence from the Uummannaq ice stream system

David H. Roberts,[1] Brice R. Rea,[2] Tim P. Lane,[1] Christoph Schnabel,[3] and Angel Rodés[3]

Received 17 April 2012; revised 7 December 2012; accepted 7 January 2013; published 2 May 2013.

[1] This paper presents the first assessment of the Uummannaq ice stream system (UISS) in West Greenland. The UISS drained ~6% of the Greenland ice sheet (GrIS) at the Last Glacial Maximum (LGM). The onset of the UISS is a function of a convergent network of fjords which feed a geologically controlled trough system running offshore to the shelf break. Mapping, cosmogenic radiogenic nuclide (CRN) dating, and model output reveal that glacially scoured surfaces up to 1266 m above sea level (asl) in fjord-head areas were produced by warm-based ice moving offshore during the LGM, with the elevation of warm-based ice dropping westwards to ~700 m asl as the ice stream trunk zone developed. Marginal plateaux with allochthonous blockfields suggest that warm-based ice produced till and erratics up to ~1200 m asl, but CRN ages and weathering pits suggest this was pre-LGM, with only cold-based ice operating during the LGM. Deglaciation began on the outer shelf at ~14.8 cal. kyrs B.P., with Ubekendt Ejland becoming ice free at ~12.4 ka. The UISS then collapsed with over 100 km of retreat by ~11.4 ka–10.8 cal. kyrs B.P., a rapid and complex response to bathymetric deepening, trough widening, and sea-level rise coinciding with rapidly increasing air temperatures and solar radiation, but which occurred prior to ocean warming at ~8.4 cal. kyrs B.P. Local fjord constriction temporarily stabilized the unzipped UISS margins at the start of the Holocene before ice retreat inland of the current margin at ~8.7 ka.

Citation: Roberts, D. H., B. R. Rea, T. P. Lane, C. Schnabel, and A. Rodés (2013), New constraints on Greenland ice sheet dynamics during the last glacial cycle: Evidence from the Uummannaq ice stream system, *J. Geophys. Res. Earth Surf.*, *118*, 519–541, doi:10.1002/jgrf.20032.

1. Introduction and Rationale

[2] Mass balance observations of the Greenland Ice Sheet (GrIS) show that it is undergoing rapid change due to direct melt losses and ice dynamic feedback, although the forcing mechanisms and controlling processes are poorly understood [*Vieli and Nick*, 2011]. Of particular importance is the behavior of marine terminating ice streams which control the majority of ice loss. Recent short-term, marine margin fluctuations have been linked to changing air and ocean temperatures [*Velicogna and Wahr*, 2006; *Holland et al*., 2008; *Joughin et al*., 2010; *Straneo et al*., 2010; *Andresen et al*., 2012; *Bjørk et al*., 2012], but this sub-decadal record of glacier change provides no firm basis to make confident predictions of ice stream response to climate forcing (decadal to centennial) [*Joughin and Alley*, 2011]. There is a need, therefore, to develop longer-term perspectives on ice sheet and ice stream behavior, in order to improve our knowledge of the environmental controls that drive GrIS dynamics

[3] In Greenland, the short-term dynamics of Jakobshavn Isbrae, Helheim, and Kangerdlussuaq glaciers have been monitored and modeled [*Echelmeyer and Harrison*, 1990; *Iken et al*., 1993; *Truffer and Echelmeyer*, 2003; *Howat et al*., 2005; *Joughin*, 2006; *Luckman et al*., 2006; *Nick et al*., 2009], but few studies have attempted to reconstruct ice stream dynamics over longer timescales [*Roberts and Long*, 2005; *Weidick and Bennike*, 2007; *Roberts et al*., 2010; *Young et al*., 2011; *Hughes et al*., 2012]. *Roberts et al*. [2010] suggested at least six regional cross-shelf troughs directed ice streams across the shelf of West Greenland during the LGM (Figure 1), but until recently, the only direct evidence for ice stream footprints offshore has come from the northeast and southeast sectors of the shelf [*Lykke-Andersen*, 1998; *Solheim et al*., 1998; *Ó Cofaigh et al*., 2004; *Evans et al*., 2009].

[4] This paper presents evidence for the Uummannaq ice stream system (UISS). The UISS drained ~6% of the Greenland ice sheet (GrIS) at the Last Glacial Maximum (LGM), and together with the adjacent Jakobshavn Isbrae ice stream system emanating from Disko Bugt, it exerted significant control on ice and water flux to the West Greenland shelf edge and into Baffin Bay during the LGM. It, therefore, played a major role in regulating GrIS internal dynamics and mass balance and would have influenced North Atlantic

[1]Department of Geography, Durham University, Durham, UK.
[2]Geography and Environment, School of Geosciences, University of Aberdeen, Aberdeen, Scotland.
[3]NERC Cosmogenic Isotope Analysis Facility, East Kilbride, UK.

Corresponding author: D. H. Roberts, Department of Geography, Durham University, Science Laboratories, Durham DH1 3LE, UK. (D.H.Roberts@durham.ac.uk)

2169-9003/13/10.1002/jgrf.20032

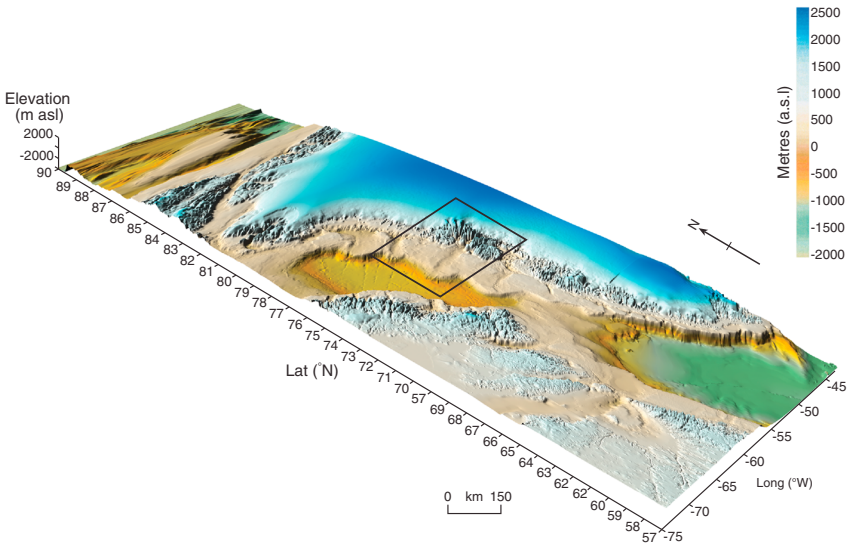

Figure 1. Topographic and bathymetric overview of West Greenland (Source: IBCAO). A number of large troughs crosscut the continental shelf, the largest of which is the Uummannaq trough (highlighted box). This reaches depths of >800 m below sea level and trends east to west to the shelf edge where it terminates in a large trough mouth fan.

thermohaline circulation. However, no previous study has considered its presence or influence on GrIS dynamics. The paper first considers the geological, geomorphological, and geochronological evidence relating to UISS flow configuration in order to reconstruct the conditions governing the southern region of the ice stream onset zone during the last glacial cycle. Second, equilibrium profile ice surface reconstructions are presented for three flow lines which drained the southern part of the UISS. In combination with the geomorphological data, these are used to provide the first constraints on the configuration of a large Greenland cross-shelf ice stream system. Finally, the forcing mechanisms driving UISS deglaciation are discussed with reference to regional changes in topography as well as atmospheric, oceanic, and sea-level forcing mechanisms.

2. Greenland Ice Sheet History

[5] Despite over 40 years of research, a number of issues continue to restrict our understanding of the longer-term dynamics of the GrIS. For example, detailed field mapping and chronology for LGM and deglacial ice extent, and especially thickness, is still limited [*Kelly*, 1985; *van Tatenhove et al*., 1996; *Bennike and Björck*, 2002; *Håkansson et al*., 2007; *Roberts et al*., 2008, 2009; *Larsen et al*., 2011], and this dearth of information is mirrored on the continental shelf [*Brett and Zarudzki*, 1979; *Ó Cofaigh et al*., 2004; *Jennings et al*., 2006; *Evans et al*., 2009; *Roberts et al*., 2010]. Furthermore, contemporary observations demonstrate that marine-based outlet glaciers and ice streams are responding asynchronously to variable ocean and climate forcing, and at a different rate to the terrestrial terminating ice sheet margins [*Rignot and Kanagaratnam*, 2006; *Holland et al*., 2008; *Joughin et al*., 2010]. However, these observations cover only decadal timescales, and it is unknown if this behavior can be upscaled. Understanding the longer-term response of ice steams to climate forcing is therefore essential as they are responsible for the bulk loss of ice to the oceans and their dynamics are largely unknown beyond very short timescales. Furthermore, contemporary observations also suggest that climate proxies cannot be directly translated to ice margin response during the last glacial cycle [*Roberts et al*., 2010].

[6] At present, all of the large GrIS ice streams are constrained by troughs (e.g., Jakobshavn Isbrae, Helheim, and Northeast Greenland Ice Stream (NEGIS) [*Bamber et al*., 2000]). Traditionally, most are thought to operate over rigid beds, with basal sliding and internal deformation controlling forward motion [*Echelmeyer and Harrison*, 1990; *Echelmeyer et al*., 1994; *Zwally et al*., 2002]. This is reflected in the development of roches moutonnées and whaleback bedforms across large tracts of former ice stream beds by mechanical erosion at the ice-bed interface [*Roberts and Long*, 2005; *Roberts et al*., 2010]. However, recent research on Jakobshavn Isbrae points to sliding over a deformable bed, and this may be applicable to many GrIS ice streams [*Block and Bell*, 2011]. In general, the controls on ice stream onset are largely unknown. Geothermal heat flux may be important for initiation of the NEGIS [*Layberry and Bamber*, 2000], although for most Greenlandic ice streams, geologic and topographic controls seem more important [*Swift et al*., 2008]. Where large troughs (formed through selective linear erosion) capture ice sheet flow, it is likely that concomitant, erosional feedback reinforces convergent flow [*Jamieson et al*., 2008; *Kessler et al*., 2008], but it is unclear how, or indeed if, ice streams existed prior to phases of selective linear erosion. It has been hypothesized that during the LGM, many contemporary ice streams and outlet glaciers currently nested within the fjord heads of the present coast, converged and flowed on to the continental shelf as large-scale composite ice streams [*Roberts and Long*, 2005; *Weidick and Bennike*, 2007], but the configuration of these systems remains poorly constrained [*Roberts et al*., 2010; *Ó Cofaigh et al*., 2013].

2.1. The Uummannaq Region

[7] The Uummannaq region is mountainous with many plateaux and summits reaching 1500–2000 m asl, and it contains some of the highest relief on the west coast of Greenland. The area is dissected by fjords which converge from east to west and route outlet glaciers/ice streams to calving margins, and during colder stages, ice out onto the shelf (Figure 2). The area straddles the low-to-high Arctic climatic transition, with mean annual air temperatures ranging from −7° to −3°C [*Box et al.*, 2006]. The relatively warm, subsurface, West Greenland Current (WGC) operates offshore (1 to 3°C; 1997–2006) [*Holland et al.*, 2008]. Geologically, the east of this region is underlain by Archaen basement rocks (~3.0–2.8 billion years old), dominated by banded gneiss (Figure 3). Overlying these in the northeast are Palaeoproterozoic volcanic and sedimentary rocks (~2.0 billion years old). A fault-bounded Cretaceous sedimentary basin runs north to south through the center of the region. To the west and northwest over the Nuussuaq Peninsula, Ubekendt Ejland, Svartenhuk, and offshore are Palaeocene volcanic rocks formed ~60 million years ago [*Chalmers et al.*, 1999].

[8] The long-term glacial history of this region is poorly known. *Sugden* [1974] defined areas of ice sheet selective linear erosion and areal scour, localized areas dissected by cirques and small outlet glaciers sourced from plateau ice caps, as well areas on the western side of Svartenhuk that appeared unglaciated. High-elevation blockfields and a lack of moraines on Svartenhuk led *Kelly* [1985] to suggest that the LGM GrIS surface was only ~450–400 m asl, with ice barely reaching the inner shelf, though the operation of ice sheet selective linear erosion provides an explanatory mechanism for blockfield cover and extensive vertical glacial

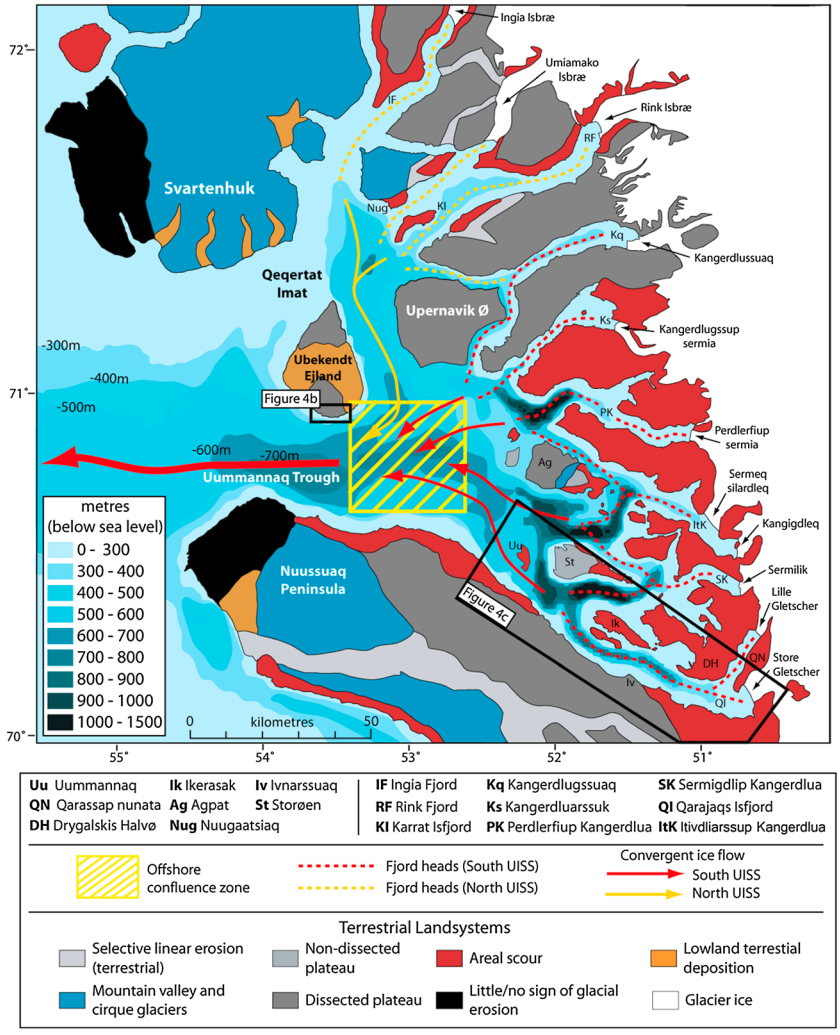

Figure 2. Landscape overview of the Uummannaq region. The terrain between Store Gletscher and Ingia Isbrae is 1500–2000 m asl and forms a dissected plateau. Regional scale flow convergence is caused by a combination of fjord head alignment and the confluence of Iglorssuit Sund and the Uummannaq trough to the SE of Ubekendt Ejland. The seafloor to the north Ubekendt is shallow (<200 m below sea level) compared to the area to the east and south, where the floors of Igdlorssuit Sund and Uummannaq trough are >800 m below sea level. The broad landscape classifications are based on recent mapping using 1:150,000 scale air photographs. Southern Ubekendt, Uummannaq, Ikerasak, Ivnarssup Qava, and Dygalskis Halvø were extensively ground truthed.

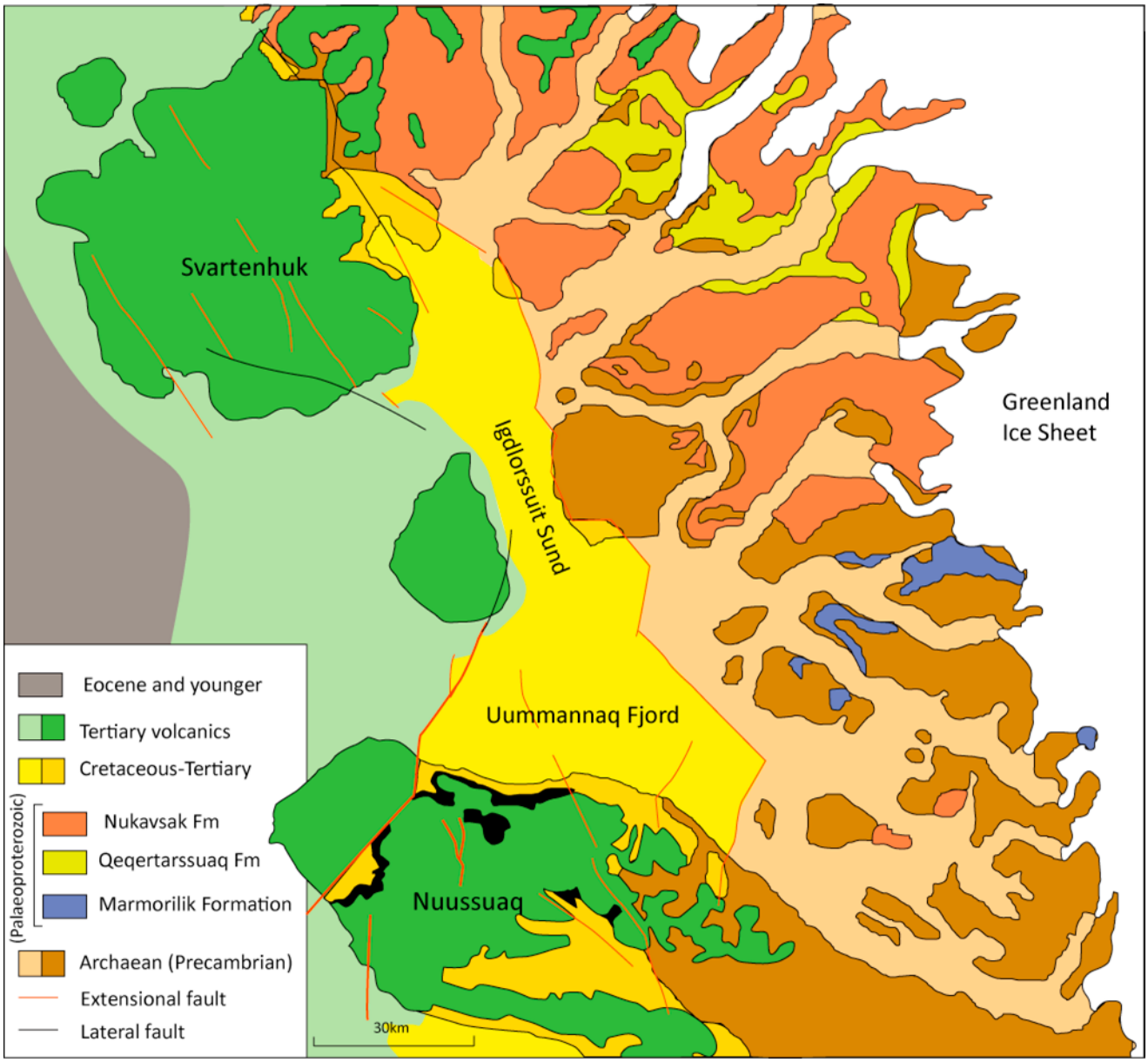

Figure 3. The geology of the Uummannaq region. Precambrian gneisses lie to the SE (~3.0–2.8 Ma), with slightly younger Palaeoproterozoic sedimentary and volcanic rocks (~2.0 Ma) to the northeast. A Cretaceous (~90–70 Ma) sedimentary basin runs N/S south from Svartenhuk to Uummannaq. The western area is buried by Palaeocene volcanic rocks (~60 Ma).

incision without the need for appeal to non-glaciation [*Nesje and Dahl*, 1990; *Rea et al*., 1996]. These interpretations of ice thickness and extent contradict recent findings further south in West Greenland which demonstrate thick ice operating on the mid-shelf to outer shelf during both MIS 2 and MIS 6 (~750+ m asl) [*Rinterknecht et al*., 2009; *Roberts et al*., 2009]. Coastal sites on western Svartenhuk have also revealed MIS 5e deposits that have been used to infer LGM ice did not inundate Svartenhuk [*Bennike et al*., 1994]. The offshore bathymetry of this region shows a cross-shelf trough which runs into a trough mouth fan at the shelf edge (Figure 1) and *Ó Cofaigh et al*. [2013] provide compelling evidence for extensive cross-shelf glaciation at the LGM. A radiocarbon date from the outer shelf shows deglaciation occurred prior to 14.8 cal. kyrs B.P. [*Ó Cofaigh et al*., 2013]. *McCarthy* [2011] reports a limiting date of 10.9 cal. kyrs B.P. for deglaciation of the mid-shelf, which is similar to deglacial dates on shells from uplifted, marine deltaic sediments from the inner coast near Patorfik and Svartenhuk (10.8 to 10.5 cal. kyrs B.P.) [*Simonarson*, 1981; *Bennike*, 2000]. This evidence broadly concurs with the concept of ice recession from the outer shelf sometime between 16 and 11 cal. kyrs B.P. [*Funder and Hansen*, 1996].

3. Methods

3.1. Geomorphology

[9] Preliminary geomorphological base maps were established using 1:150,000 scale aerial photographs (1985; KMS, Denmark). These were ground truthed and supplemented by

extensive field mapping, particularly along a corridor from Store Gletscher westwards to Ubekendt Ejland (Figure 2). Abraded bedrock, roches moutonnées, and striae were mapped in order to reconstruct basal ice flow patterns using established criteria for the identification of subglacial erosional features [*Gordon*, 1981; *Glasser and Warren*, 1990; *Sugden et al*., 1992; *Roberts and Long*, 2005]. Moraines, deltas, and eskers were mapped to establish the nature and timing of ice advance and retreat from the outer to inner coast. Trimlines were identified as limits separating glacially eroded terrain from shattered periglacial blockfield areas [*Kelly*, 1985; *Ballantyne*, 1997] though in all instances, these were transitional rather than clear linear boundaries. To test whether trimlines represented former ice sheet surface altitudes, englacial thermal boundaries (with upper blockfields being protected by cold ice), or postglacial weathering limits, samples were collected for CRN analyses to establish exposure and burial histories [*Bierman et al*., 1999; *Marsella et al*., 2000; *Briner et al*., 2006; *Phillips et al*., 2008]. Altitudes are expressed in meters above present sea level (m asl) and have a precision of ±10 m determined by a handheld GPS.

3.2. Cosmogenic Radionuclide (CRN) Exposure Dating

[10] Samples for CRN dating were collected from in situ, glacially abraded bedrock surfaces and large, sub-glacially modified erratics (typically >2 m^3) from five vertical sampling profiles along a 150 km transect from the contemporary margin of Store Gletscher to Ubekendt Ejland in order to determine ice stream geometry and the chronology of ice retreat and thinning from the LGM (Figures 2 and 4a–4c). The samples span an altitudinal range from ~ 40 to 1250 m asl and include bedrock and erratic samples collected from above and below trimlines, blockfields, and glacially abraded terrain. Samples were taken using a rock cutting saw and comprise a mixture of quartz gneiss, granites, and micro-diorites. Sampling protocols followed

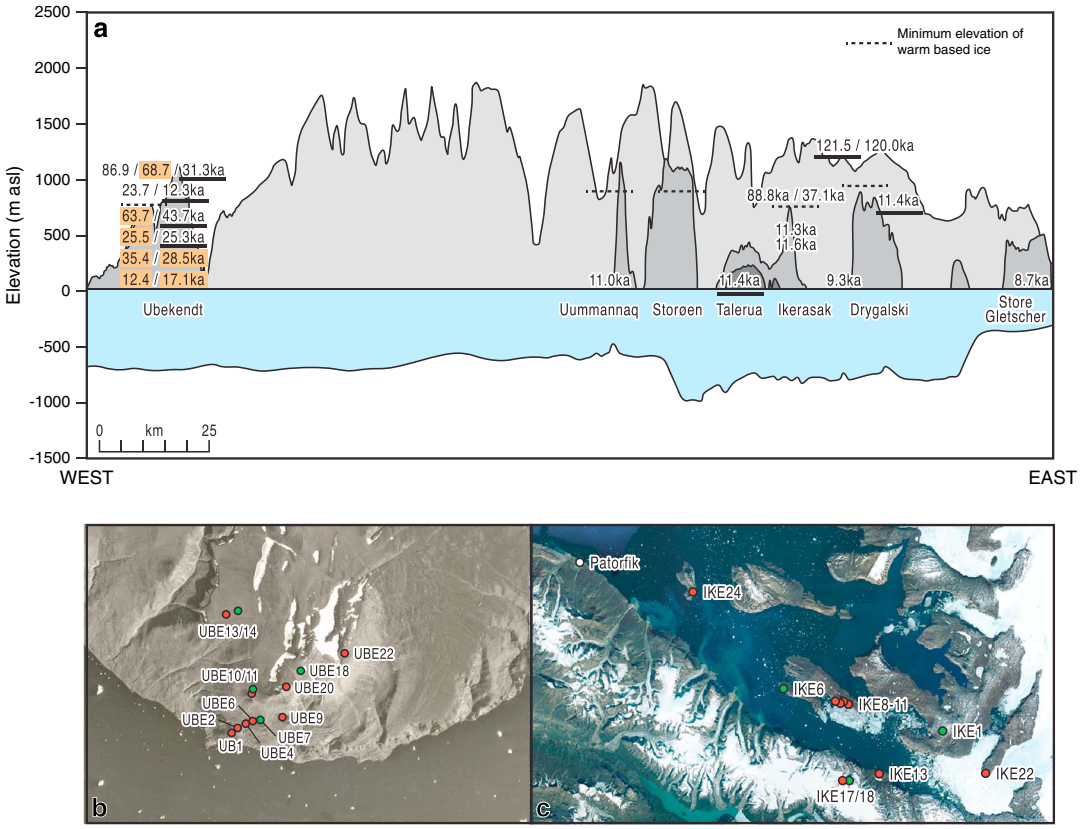

Figure 4. (a) Topographic and bathymetric cross section of the Uummannaq trough between Store Gletscher in the east and Ubekendt Ejland in the west. Definitive evidence for warm-based ice (i.e., scoured terrain) can be found at ~966 m asl in the east on Drygalskis Halvø, but this limit drops westward down to ~700 m asl on Ubekendt Ejland. On Nuussuaq and Ubkendt, both bedrock and erratics suggest complex exposure histories with cold-based ice protecting areas above 700 m asl during the last glacial cycle. On Ubekendt two CRN ages suggest that below ~770 m asl the island may have deglaciated between 12.4 and 12.3 ka; however, the CRN profile does not young sequentially with elevation pointing to complex differential erosion and inheritance of erratic and bedrock surfaces. Consistent CRN ages of ~11 ka on Uummannaq and Ikerasak suggest retreat of the UISS from Ubekendt Ejland between 12.4 and 11 ka, with a slower retreat rate between Ikerasak and Store gletscher at the start of the Holocene (9.3–8.7 ka). Be CRN ages in black; chlorine CRN ages highlighted in orange; erratic samples underlined; all other samples from bedrock. (b) The location of CRN samples on southern Ubekendt Ejland. (c) The location of CRN samples between Uummannaq and Store Gletscher. Erratic samples—green. Bedrock samples—red.

Table 1. Sample Location, Altitude, Shielding, and Thickness

Sample Code	Lat (N)	Long (W)	Alt (m asl)	Sample Type	Shielding Factor	Effective Thickness (g cm^{-2})
UBE 1	71.03	53.69	122	Bedrock	0.9837	11.23
UBE 2	71.03	53.68	233	Bedrock	0.9906	10.54
UBE 4	71.03	53.68	352	Bedrock	0.9881	11.21
UBE 6	71.03	53.66	463	Bedrock	0.9955	8.03
UBE 7	71.04	53.66	485	Erratic	0.9905	10.10
UBE 9	71.04	53.64	597	Bedrock	0.9996	29.91
UBE 10	71.04	53.67	682	Bedrock	0.9939	19.27
UBE 11	71.05	53.67	688	Erratic	0.9864	9.84
UBE 13	71.07	53.69	756	Bedrock	0.9977	10.27
UBE 14	71.07	53.68	770	Erratic	0.9989	13.06
UBE 18	71.06	53.64	975	Erratic	0.9994	9.83
UBE 20	71.05	53.65	1012	Bedrock	1.0000	14.53
UBE 22	71.06	53.61	1142	Bedrock	1.0000	8.77
IKE 1	70.46	50.90	956	Erratic	0.9997	12.48
IKE 6	70.54	51.70	129	Erratic	0.9858	9.35
IKE 8	70.51	51.38	810	Bedrock	0.9999	10.85
IKE 9	70.51	51.38	807	Bedrock	0.9996	9.75
IKE 10	70.51	51.40	642	Bedrock	0.9934	7.84
IKE 11	70.52	51.41	497	Bedrock	0.9961	12.02
IKE 13	70.39	51.18	163	Bedrock	0.9962	10.12
IKE 17	70.38	51.33	1170	Bedrock	0.9597	9.48
IKE 18	70.38	51.33	1182	Erratic	0.9992	11.01
IKE 22	70.39	50.68	39	Bedrock	0.9638	12.18
IKE 24	70.69	50.13	120	Bedrock	0.9951	13.74

Roberts et al. [2008, 2009], and all details are presented in Tables 1 and 2.

3.2.1. Sample Preparation

[11] Quartz-rich samples were processed for ^{10}Be/^{26}Al measurement in quartz. The rest of the samples were prepared for ^{36}Cl determination in bulk rock. The sample preparation and ^{10}Be/^{26}Al measurement procedures used in this study are described in detail in *Wilson et al*. [2008] and *Ballantyne et al*. [2009]. In this project, between 130 and 220 μg Be was added as carrier per sample. Inherent Al concentrations in quartz were determined with an ICP-MS at Scottish Universities Environmental Research Center (SUERC). The relative standard uncertainty of this determination was 3%. Al carrier was added to most samples so that 1.6 mg Al per sample was reached.

[12] Samples for ^{36}Cl were crushed, sieved to 125–250 μm, and leached in hot 2 M HNO_3 to remove meteoric ^{36}Cl contamination. Each sample was then split into two fractions: ~2 g for elemental analysis and ~20 g for analysis of ^{36}Cl using an accelerator mass spectrometry (AMS). Chlorine was extracted and purified to produce AgCl for AMS analysis according to the procedures described in *Vincent et al*. [2010]. A high ^{35}Cl/^{37}Cl carrier was used to determine the total Cl concentration by AMS Isotope Dilution technique (AMS-ID) [*Di Nicola et al*., 2009].

3.2.2. ^{10}Be, ^{26}Al, and ^{36}Cl measurements and exposure age calculation

[13] The measurement procedures at the SUERC AMS are described in detail in *Maden et al*. [2007] and *Roberts et al*. [2008]. The sea-level high latitude ^{10}Be spallogenic production rate value used was of 3.98 ± 0.24 atoms g a^{-1}e [*Briner et al*., 2012]. Exposure ages were calculated using the CRONUS-Earth online calculator (using "NE North America—*Balco et al*., 2009" calibration data set. St scaling scheme. Trace string: Calc date: 06 July 2009. Versions: Cal 2.2-cal-dev P10fit 2.2-dev Get-age 2.1 Muons 1.1 Consts 2.2.). Attenuation correction for sample thickness uses an attenuation length of 160 g cm^{-2}. Topographic shielding correction is determined according to *Dunne et al*. [1999]. The exposure ages are not corrected for past geomagnetic field variations. Including a simple palaeomagnetic correction [*Nishiizumi et al*., 1989] results in ages ~1% older than those presented for the samples with an exposure age of about 10 ka. Age determinations include a correction for pressure related to the altitude, latitude, and longitude according to the mean global surface pressure field of the NCEP-NCAR re-analysis (www.cdc.noaa.gov/ncep_reanalysis/) but assume the standard atmosphere for geographical scaling of the production rate. Plots of our ^{26}Al/^{10}Be ratios versus ^{10}Be concentrations show that all but two of our exposure ages (UBE 13; IKE 8) fall within a 2 sigma error range of the theoretical erosion island envelope, and there is approximate concordance in ^{26}Al and ^{10}Be ages (Table 2). All CRN ages are given in thousands of years (ka) (meaning thousands of years before sample collection; AD 2008) [*Balco et al*., 2008; *Roberts et al*., 2008]. Radiocarbon ages are given as calibrated (mid-point) years before present (cal. kyrs B.P.).

[14] The model of *Schimmelpfennig et al*. [2009] was used to calculate ^{36}Cl ages. Local scaling factors were calculated from the latitude and elevation using the *Stone* [2000] scheme. Sample composition was determined by prompt-gamma (neutron) activation analysis (PGAA) and coupled plasma optical emission spectrometry (ICP-OES). Total Cl concentration was also measured by AMS-ID. According to the *Schimmelpfennig et al*. [2009] model, ^{36}Cl in studied samples is mainly produced by spallation of Ca (~45%) and capture of thermal and epithermal neutrons by ^{35}Cl (~40%). For simplicity, only Be and Cl ages are shown in Figure 4 and boulder samples are underlined.

3.3. Ice Sheet Equilibrium Profile Reconstructions

[15] Two equilibrium models are applied for the reconstruction of the UISS. Model 1 assumes a "perfectly plastic"

Table 2. ^{10}Be, ^{26}Al, and ^{36}Cl Cosmogenic Exposure Ages for the UISS

Sample Code	ID for ^{10}Be AMS	^{10}Be (at g^{-1})	Sigma ^{10}Be (at g^{-1})	Muog[c] Prod[n] Rate (at g^{-1} yr^{-1})	Spall[c] Prod[n] Rate (at g^{-1} yr^{-1})	^{10}Be Exp Age (years) No Erosion	Internal Uncert[y] (year)	External Uncert[y] (year)
^{10}Be calculations								
UBE 7	b4161	1.82×10^5	6.30×10^3	0.218	6.56	25,302	860	2319
UBE 11	b4445	3.46×10^5	1.22×10^4	0.234	7.94	43,778	1526	4044
UBE 13	b4668	2.03×10^5	7.22×10^3	0.24	8.55	23,778	831	2188
UBE 14	b4456	1.06×10^5	4.7×10^3	0.241	8.6	12,304	535	1175
UBE 18	b4457	3.26×10^5	1.22×10^4	0.259	10.47	31,355	1159	2915
UBE 22	b4160	1.13×10^6	3.94×10^4	0.275	12.18	86,932	3015	8100
IKE 1	b5010	1.16×10^5	3.39×10^3	0.257	10.2	11,402	326	1020
IKE 6	b4430	5.28×10^4	2.15×10^4	0.191	4.53	11,470	460	1077
IKE 8	b4444	7.84×10^5	2.73×10^4	0.244	8.98	88,836	3099	8287
IKE 9	b4450	3.32×10^5	2.73×10^4	0.244	8.99	37,163	3020	4420
IKE 10	b4667	8.76×10^4	3.50×10^3	0.23	7.7	11,317	444	1059
IKE 11	b5025	7.77×10^4	2.76×10^3	0.218	6.64	11,634	405	1067
IKE 13	b5011	4.51×10^4	1.31×10^3	0.193	4.75	9360	268	837
IKE 17	b4427	1.39×10^6	4.52×10^4	0.277	11.94	120,031	3928	11,175
IKE 18	b4428	1.47×10^6	5.12×10^4	0.278	12.5	121,589	4257	11,429
IKE 22	b4159	3.88×10^4	2.04×10^3	0.185	3.98	8729	450	869
IKE 24	b5026	5.03×10^4	3.73×10^3	0.19	4.46	11,083	807	1248

^{26}Al calculations Sample code	ID for ^{26}Al AMS	^{26}Al (at g^{-1})	Sigma ^{26}Al (at g^{-1})	Muog[c] Prod[n] Rate (at g^{-1} yr^{-1})	Spall[c] Prod[n] Rate (at g^{-1} yr^{-1})	^{26}Al Exposure Age (years) no erosion	Internal Uncert[y] (year)	External Uncert[y] (year)	^{26}Al/^{10}Be (at at -1)	Sigma ^{26}Al/^{10}Be (at at -1)
UBE 7	a1235	1.06×10^6	4.30×10^5	1.817	44.26	23,943	956	2264	6.40	0.34
UBE 13	a1335	2.64×10^5	1.44×10^4	2.004	57.67	4540	243	457	1.30	0.08
UBE 14	a1278	7.69×10^5	3.54×10^4	2.01	57.99	13,193	599	1276	7.26	0.46
UBE 18	a1276	2.37×10^6	1.18×10^5	2.167	70.63	33,919	1686	3380	7.28	0.45
UBE 22	a1234	6.73×10^6	2.69×10^5	2.3	82.2	85,429	3467	8308	6.53	0.35
IKE 8	a1267	4.46×10^6	1.70×10^5	2.041	60.61	75,631	292	6624	5.70	0.29
IKE 9	a1277	2.39×10^6	7.93×10^4	2.041	60.63	39,793	1316	3676	7.2	0.64
IKE 17	a1265	8.89×10^6	3.33×10^5	2.32	80.57	116,076	4491	11,339	6.39	0.32
IKE 18	a1263	8.99×10^6	3.59×10^5	2.327	84.36	111,942	4620	11,040	6.09	0.32

^{36}Cl calculations Sample Code	ID for ^{36}Cl AMS	Cl Conc[n] [ppm]	Cl-36 Conc[n] ^{36}Cl [atoms/g]	^{36}Cl Prod[n] Rate Atoms ^{36}Cl g^{-1} a^{-1}	^{36}Cl Exposure Age (years)	Internal Uncert[y] (years)	External Uncert[y] (years)
UBE1	c2412	210.0 ± 11.6	$207{,}034 \pm 31{,}186$	12.29 ± 0.15	17,178	±2649	±2958
UBE2	c2413, c2414	82.8 ± 6.6	$136{,}577 \pm 25{,}769$	11.11 ± 0.34	12,471	±2419	±2583
UBE4	c2415	244.6 ± 18.7	$512{,}499 \pm 45{,}034$	18.51 ± 0.34	28,595	±2655	±3422
UBE6	c2416	54.2 ± 2.3	$395{,}528 \pm 28{,}742$	11.61 ± 0.33	35,469	±2890	±3960
UBE9	c2423	163.9 ± 8.8	$502{,}750 \pm 24{,}265$	20.30 ± 0.17	25,501	±1287	±2311
UBE10	c2424	90.6 ± 3.2	$771{,}594 \pm 28{,}865$	13.01 ± 0.13	63,749	±2656	±5655
UBE20	c2425,c2426	7.6 ± 0.5	$838{,}376 \pm 26{,}735$	13.19 ± 0.43	68,738	±3391	±6935

ice rheology, and the solution provided by *Van der Veen* [1999] is solved numerically using the spreadsheet model "Profiler" of *Benn and Hulton* [2010]:

$$h_{i+1}^2 - h_{i+1}(b_i + b_{i+1}) + h_i(b_{i+1} - H_i) - \frac{2\Delta x \bar{\tau}_b}{\rho g} = 0 \quad (1)$$

where h is the ice surface elevation, H is the ice thickness, b is the bedrock elevation, Δx is the step length, $\bar{\tau}_b$ is the basal shear stress (equal to the yield stress) averaged over the step interval, ρ is the density of ice, g is gravity, and i is the ith step. The only inputs required for this model are the bed elevation, location of the ice margin, and the ice divide. The shear stress is tuned until a fit to the geomorphology observed in the field is obtained.

[16] Model 2 is a Weertman-sliding profile [*Schilling and Hollin*, 1981; *Van der Veen*, 1999] which is again solved numerically:

$$h_{i+1} = h_i + \frac{A[a(L - \Sigma\Delta x)]^{1/m}}{\rho g H_i^{1+(1/m)}}\Delta x \quad (2)$$

where A^{-m} is a sliding constant ($=\tau^{-m}u$), a is accumulation rate, L is the distance from the ice margin to the ice divide, $\Sigma\Delta x$ is the distance along the flow line, m is the sliding exponent (2.5, following *Schilling and Hollin* [1981], and u is the sliding velocity, with everything else as above. This model is suitable for ice masses where there is a significant component of mass loss via calving, ice velocities (and sliding) are high and remain so to the ice edge [*Schilling and Hollin*, 1981], which are reasonable assumptions for the UISS. Neither Model 1 nor Model 2 has a shape factor included so an infinitely wide glacier geometry is assumed. This is reasonable for the ice sheet interior and also for the outer fjord and shelf areas where trough sides are only a minor component of the overall ice-bed contact area (high width to depth ratio). However, it is less realistic for the inner fjord sections between Ubekendt Ejland and the present ice margin. This is compensated for by using a higher value for the basal shear stress in Model 1 and the sliding constant in Model 2. The absolute values for both, provided they are within reasonable limits, are of no major concern because the ice surface is constrained by the geomorphology observed in the field. These two models have been applied specifically to compare ice surface profiles beyond the inner fjord where we have no empirical control data. Model 1 is the least tuneable and has known errors in the ice sheet interior, while Model 2 will likely produce the most realistic ice surface. The lack of treatment of grounding line dynamics in either model is negated as the ice surface elevation is fitted to the geomorphology, and these are equilibrium profile and not dynamic models. Any errors in the initial calving margin thickness will have negligible effect on the geometry even a short distance up-flow from the grounding line.

[17] Fjord bathymetry comes from the GEBCO_08 Grid, and the ice sheet bed topography comes from the CReSIS bed elevation DEM. The DEMs were merged along the present ice sheet margin, and the CReSIS data were found to be erroneous around the calving margin of Store Gletscher where it appeared to rise above sea level. The bed, just distal from the present ice margin of Store Gletscher for 33 km up-flow line, has been modified to account for this by mirroring the gradient of the ice surface, to an inflection point in the present ice sheet surface. The present-day ice surface is taken from *Bamber et al*. [2001, 2001].

4. Results

4.1. Regional Topography and Geology

[18] The eastern Uummannaq region is characterized by deep coastal fjords (cut through the Archaen and Proterozoic basement) that route outlet glaciers and ice streams to calving margins at the coast. The fjord terrain can be classified into areas of ice sheet selective linear erosion and areal scour, those that have undergone glaciation by small ice caps, valley, and cirque glaciers prevalent in higher-elevation mountains and, finally, high-elevation plateau terrain with ice fields above ~1200 m asl (Figure 2).

[19] Two large submarine troughs characterize the offshore area immediately west of the fjords. The Uummannaq trough reaches depths of 600–1000 m running westwards from Store Gletscher to Uummannaq and south of Ubekendt Ejland where it is ~600–800 m deep. Igdlossuit Sund is ~500–600 m deep and trends north-south through a Cretaceous fault-bounded basin which feeds into the Uummannaq trough from the north (Figures 2 and 3). In the southern sector of the Uummannaq region, six inner coast fjords converge into the confluence area of the Uummannaq trough and Igdlossuit Sund (Figure 2). Average fjord wall elevation varies between 1180 and 1894 m asl, and they range in depth from 570 to 1287 m (Table 3). Further offshore, the Ummannaq trough continues to the shelf edge where it terminates in a trough

Table 3. Fjord Locations and Characteristics in the Uummannaq Region

Fjord	Mouth Location	Snout Location	Orientation (°)	Length (km)	Ave. Width at SL (km)	Ave. Plateau Height (m asl)	Max. Water Depth (m)
Kangerdlugssuaq	71°23′N 53°00′W	71°27′N 51°23′W	263	61.7	4.2	1894	570
Kangerdluarssuk	71°08′N 52°18′W	71°15′N 51°31′W	244	34.9	5.7	1671	770
Perdlerjiup Kangerdlua	71°03′N 52°00′W	70°59′N 50°57′W	282	42.5	5.5	1388	1246
Itivdliarssup Kangerdlua	70°59′N 51°58′W	70°48′N 51°00′W	302	42.5	5.6	1332	844
Sermigellip Kangerdlua	70°42′N 51°31′W	70°37′N 50°38′W	291	38.2	4.5	1180	1287
Qarajaqs Isfjord	70°41′N 52°17′W	70°22′N 50°36′W	302	75.4	6.9	1308	956

Figure 5. (a) Areally scoured terrain on Drygalski Halvø (960 m asl) looking west across Ikerasak (Ik) and the Nuussuaq Peninsula (Nq), Storøen (Sn), and Uummannaq (UU). (b) Perched sub-glacial erratic situated on areally scoured terrain on Drygalski Halvø (DH) (e.g., Sample IKE 1; 11.4 ka; Table 2).

mouth fan (Figure 1). Just east of the fan edge, it shallows to ~400–500 m deep across a distinct bank inferred to be a terminal moraine complex [*McCarthy*, 2011; *Ó Cofaigh et al.*, 2013]. To the NW of Ubekendt Ejland, the bathymetry is shallow (<200 m) with a Tertiary basalt rock sill running north onto the Svartenhuk Peninsula.

4.2. The Southern Sector of the UISS: Geometry and Chronology

4.2.1. Fjord Heads: Store and Lille Gletscher

[20] In the vicinity of Lille Gletscher and Store Gletscher areally scoured terrain extends up to 966 m asl across Drygalskis Halvø and Qarassap nunata indicating both glaciers overtopped their troughs at some point (Figures 2, 4, and 5a). The Archaen bedrock is striated (284–298°), and roches moutonnées are common. Erratics are prevalent, often perched, and show evidence of sub-glacial transport (i.e., striated and sub-angular/sub-rounded; Figure 5b). Sample IKE 1 taken from a perched erratic produced a CRN exposure age of 11.4 ka for the deglaciation of this terrain (Table 2 and Figures 4a and 4c). This style of fjord submergence and high-level areal scouring extends north to Perdlerjiup Kangerdlua where areal scour is evident up to 1100 m asl (Figure 2). At the margin of Store Gletscher, a scoured and striated bedrock sample taken from just above the marine limit yielded a ^{10}Be age of 8.7 ka (IKE 22; Tables 1 and 2 and Figure 4).

4.2.2. Inner Fjords: Ivnarssup Qava on the Nussuuaq Peninsula

[21] Between Store Gletscher and Ivnarssuaq, the terrain flanking the fjord is ice scoured up to ~750 m asl (Figure 2). Above this however, in ground-truthed locations, the landscape is composed of frost-shattered gneissic bedrock and blockfield with occasional erratics. Two low relief surfaces are apparent above ~750 m asl and another above ~1150 m asl. Sample IKE 13 (^{10}Be) taken from a low-elevation, striated, bedrock site (163 m asl) along the northern shore of Ivnarssuaq yielded an Early Holocene deglacial age of 9.3 ka (Figure 4c and Table 2). In places along the upper edge of fjord walls (e.g., Ivnarssuaq; 750 m asl), there is evidence for ice overtopping the trough onto the lower blockfield mantled surface. This has resulted in the bulldozing of blockfield material to reveal bare bedrock surfaces and the production of push moraines (Figures 6a and 6b). The moraines are thus dominated by local lithology with occasional erratics.

[22] The blockfields are intriguing and although not the focus of this paper are briefly mentioned. On the edges of the cliffs, in situ weathering exceeding 2 m deep is clear (Figures 6c and 6d). However, a significant proportion of the surface boulders are sub-angular (SA) to sub-rounded (SR) though their frequency diminishes with elevation. Excavations were made in four pits in the blockfields, two on the lower surface (~750–850 m asl) and two on the upper (above ~1200 m asl). Numerous SA and SR clasts were found, and the matrix in all instances was sandy. Overall, these observations led to an interpretation that these blockfields are dominantly allochthonous, formed from pre-existing till cover with some additional input of in situ-heaved bedrock blocks [*Dahl*, 1966]. Weathering pits and runnels on both in situ bedrock and erratic surfaces suggest that the plateau may have been sub-aerially exposed for some considerable time (Figure 6f), and this is supported by CRN ages. Sample IKE 17 taken from an in situ bedrock outcrop has a ^{10}Be age of 120.0 ka and a ^{26}Al age of 116.1 ka. Sample IKE 18, taken from an erratic with surface weathering pits, mirrored this with a ^{10}Be age of 121.5 ka and a ^{26}Al age of 111.9 ka (Figure 4 and Table 2).

4.2.3. Inner Fjords: Ikerasak

[23] The lower flanks of Ikerasak are streamlined with areas of closely spaced roches moutonnées (Figure 7a). Sample IKE 6 (^{10}Be), a low-elevation (129 m asl) perched erratic on the west end of Talerua, provided an exposure age of 11.4 ka (Figure 4 and Table 2). Sample IKE 10 (^{10}Be), a leeside roche moutonnée bedrock site on the eastern end of Ikerasak (642 m asl), provided an exposure age of 11.3 ka, while IKE 11 (^{10}Be), a mid-stoss roche moutonnée sample, provided an age of 11.6 ka (497 m asl) (Figure 4c and Table 2). Above ~750 m asl, the evidence for warm-based ice scour is less clear. The summit of Ikerasak (~825 m asl) has crude,

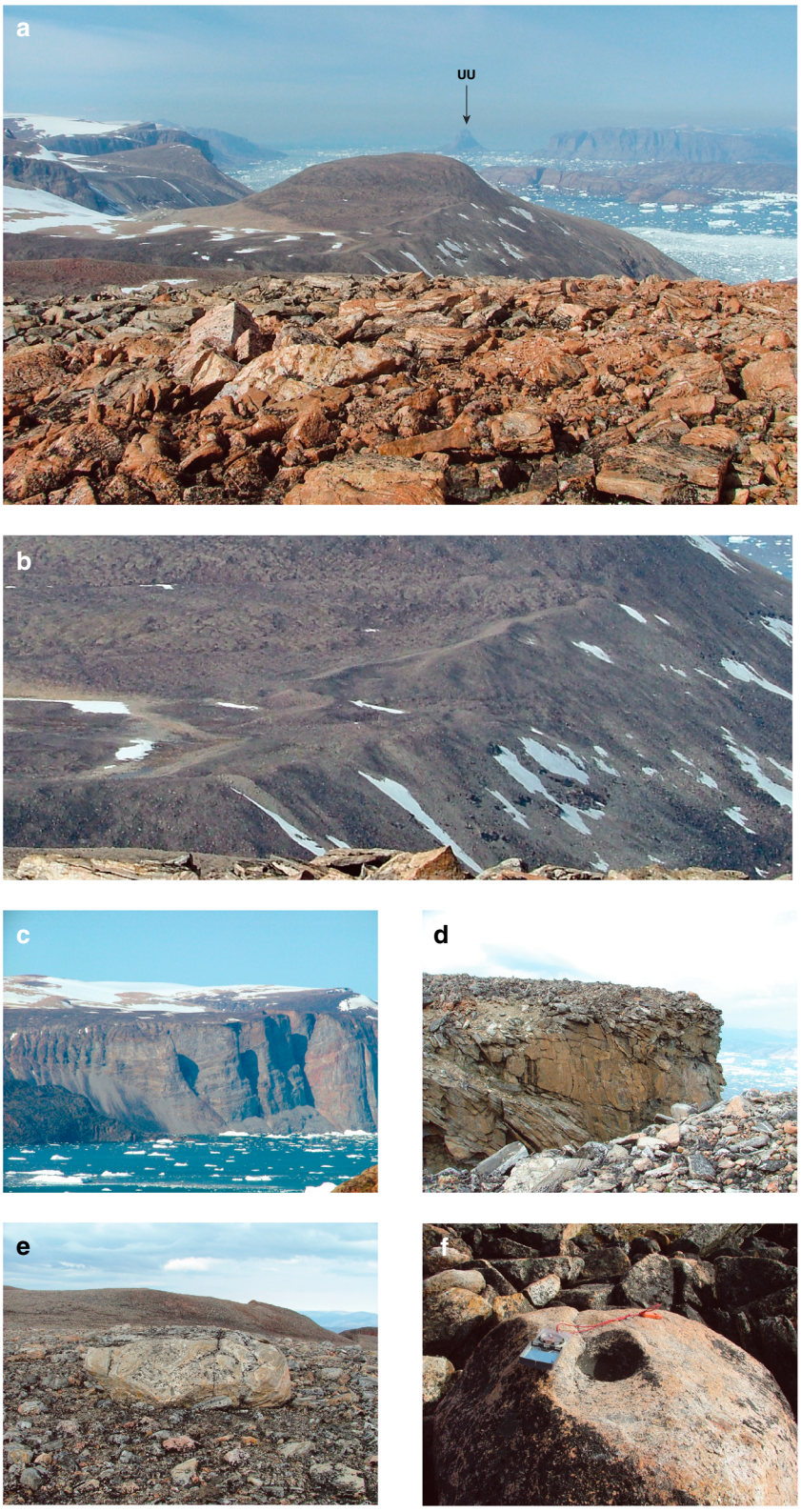

Figure 6. (a) The upper surface of the northern edge of the Nuussuaq Peninsula looking west towards Uummannaq. Note the angular blockfield terrain and undulating topography. (b) Along the edge of the plateau, push moraines can be seen overtopping the plateau edge (~750–800 m asl). (c) Below ~750 m asl, the wall of the fjord are clearly glacially scoured. (d) The blockfield on the plateau is derived from ~2 m of in situ shattered bedrock (field of view ~40 m wide), though erratics up to 2 m in diameter can be found on the blockfield between 750 and 1200 m asl (e), some of which exhibit weathering pits (f).

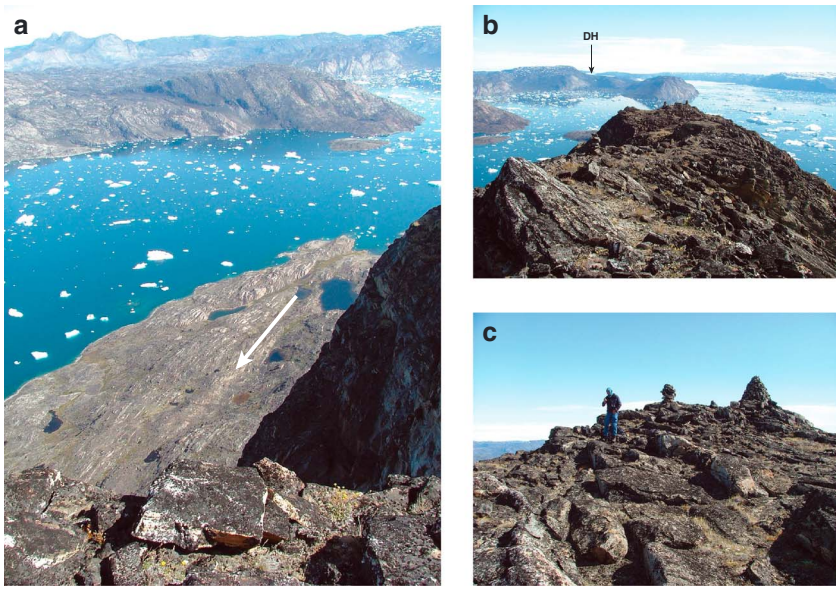

Figure 7. (a) Streamlined bedrock bedforms on the NW coast of Ikerasak, indicative of warm-based, basal sliding with ice flowing east to west (white arrow). (b) Eastern summit area of Ikerasak (~825 m asl) looking east over to Drygalski Halvø. Unlike Drygalski Halvø (~960 m asl; Figure 4a), this terrain is not clearly glacially scoured. (c) The western summit area of Ikerasak exhibiting crude plucking but little glacial scour.

Figure 8. (a) High-elevation terrain (~1000 m asl) on Ubekendt Ejland. The foreground is composed of frost-shattered granophyric bedrock. The tor is composed of micro-diorite. (b) Quartzite erratic over 2 m in diameter resting on patterned ground composed of granophyric blockfield (Sample UBE 18; 975 m asl; Table 2). (c) Large tabular striated erratic at ~900 m asl on Ubekendt Ejland (2 m diameter; lithology unknown).

hummocky, sub-angular bedrock surfaces and areas that appear to have undergone minor plucking (Figures 7b and 7c). However, there is no pronounced development of roches moutonnées, abraded surfaces, or striae, suggesting that above ~750 m asl, the island has only suffered minor sub-glacial erosion. Two samples, IKE 8 and IKE 9, both in situ bedrock samples at 810 and 807 m asl, yielded contrasting exposure histories. IKE 8 has a ^{10}Be age of 88.8ka and a ^{26}Al age of 75.6 ka, while IKE 9 has ^{10}Be age of 37.1 ka and a ^{26}Al age of 39.7 ka (Figure 4 and Table 2).

4.2.4. Inner Fjords: Storøen and Uummannaq

[24] The eastern end of Storøen is glacially scoured up to ~750–800 m asl, with abundant roches moutonnées and perched erratic boulders. Above this, the terrain rises to a split-level plateau with a lower surface ~1000–1100 m asl and a higher surface ~1200–1400 m asl (Figure 2). Both plateaux harbor a small ice cap and are mantled by blockfield, although it was not possible to verify whether this was allochthonous or autochthonous. Glacially scoured terrain on Uummannaq reaches up to 450 m asl. Above this, the slopes become very steep and prone to rock fall. IKE 24, a bedrock, sample from 120 m asl on the southern flanks of Uummannaq island provided a CRN ^{10}Be exposure age of 11.0 ka (Figure 4c and Table 2).

4.2.5. Outer Coast: Ubekendt Ejland

[25] The southern end of Ubekendt Ejland terrain above ~1090 m asl has an autochthonous blockfield cover. In three shallow pits (<0.84 m), the original bedrock structure can be discerned in the roots of weathering the profiles, but increasing levels of breakdown and heave (mixing) are evident up-profile in both granophyre and micro-diorite lithologies. Frost-shattered tors occur at high elevations (~1000 m asl; Figure 8a). They occur best in micro-diorite, but they are also found in a much more denuded state in granophyric lithologies. Above ~900 m asl where the slope angles are sufficient, the blockfield cover has been modified significantly by solifluction/gelifluction slope movements.

[26] Between ~700 and 800 m asl, there is a till covering which has been modified by frost heave to form allochthonous blockfield. Erratics are found on the blockfield and till cover between ~700 and 975 m asl (Figures 8b, and 8c). CRN samples on bedrock and erratics above 700 m asl provide a range of ages. The oldest are from the granophyre summit on the south of the island with UBE 22 (1142 m asl), a bedrock sample, having a^{10}Be age of 86.9 ka and an ^{26}Al age of 85.2 ka. Just below the summit, UBE 20 (bedrock; 1012 m asl) has a ^{36}Cl age of 68.7 ka. Erratics provide both pre-LGM and deglacial ages. UBE 18, a large flat lying quartzite boulder sitting on blockfield (975 m asl), provided a ^{10}Be age of 31.3 ka and a ^{26}Al age of 33.9 ka (Figures 4b and 8b and Table 2). UBE 14 (770 m asl), a granite erratic sitting on frost re-worked till, yielded a^{10}Be age of 12.3 ka and a ^{26}Al age of 13.1 ka. UBE 13, a quartzite boulder close to UBE14 (756 m asl) provided a^{10}Be age of 23.7 ka and a ^{26}Al age of 4.5 ka. UBE 11, a quartzite boulder located amongst partially abraded bedrock and sitting on micro-dioritic blockfield (688 m asl) has a ^{10}Be age of 43.7 ka (Figure 4 and Table 2).

[27] Below ~700 m asl, the terrain is characterized by glacially abraded bedrock, erratics, and a drape of sediment re-worked downslope by periglacial slope processes. An inset sequence of lateral moraines extends from ~670 m asl to 125 m asl. They are composed of coarse diamictic material and have sub-horizontal across slope profiles (Figures 9a–9c). Similar flights of lateral moraines have been observed elsewhere in the fjord system, for example, on Upernivik Ø and Nugatsiaq, and are best preserved in protected enclaves in the topography (Figure 2). CRN analyses on samples taken below 700 m asl have a range of ages. UBE 1 to UBE 10 range in elevation from 122 to 682 m asl. They produce a complex range of ^{10}Be, ^{26}Al, and ^{36}Cl ages that do not decrease sequentially with elevation (Figure 4). The oldest ^{36}Cl age is UBE 10 (682 m asl) at 63.7 ka. UBE 9 to UBE 4 (^{10}Be and ^{36}Cl ages; 597–352 m asl) vary in age between 35.4 and 25.3 ka. UBE 1 and UBE 2 (^{36}Cl ages; 122 and 233 m asl) provide the youngest exposure ages of 17.1 and 12.4 ka, respectively.

4.3. LGM Ice Surface Reconstruction

4.3.1. Landscape Interpretation

[28] Using the field evidence and CRN ages, it is possible to reconstruct the extent of warm and cold-based ice, minimum ice stream surface elevation, and a retreat chronology for the UISS. In the east around the fjord heads, erosional scour across Drygalski Halvo points to warm-based ice operating up to 966 m asl which deglaciated at 11.4 ka. At lower elevation, the UISS retreated east of the present margin of Store Gletscher at 8.7 ka (Figure 4 and Table 2). Moving westward, geomorphology and CRN data show erosional scour and warm-based ice operating up to 750–800 m asl along the flanks of Ivnarssup Qava and on Ikerasak, Storøen, and Uummannaq at the LGM with deglacial exposure ages range between 11.9 and 11.0 ka (Figure 4). The summit of Ikerasak (~825 m asl) was not heavily abraded suggesting it was close to the upper limit of warm-based ice (resulting in a partially inherited cosmogenic signal; Figure 4).

[29] High-elevation plateaux bordering these islands and the Uummannaq trough are characterized by allochthonous blockfield. The long-exposure ages suggest the till in which these allochthonous blockfields formed is pre-LGM in age; hence, terrain above 750–800 m asl was either ice free during the LGM or covered by cold-based ice. Given that local cold-based ice caps still cover the Nussuuaq Peninsula above 1200 m asl, it is entirely feasible that this high elevation terrain was covered by cold-based ice at the LGM, although the concordant ^{26}Al/^{10}Be ages on Nussuuaq do not support an excessively long burial period. In order to get significant non-concordant ^{26}Al/^{10}Be ages a surface must have been buried for more than a hundred thousand years.

[30] On Ubekendt, the geomorphology and geochronology are complex. The two youngest CRN ages (UBE 14 and UBE 2; Table 2), as well as the low-elevation areal scour and the lateral moraine staircase, point to post-LGM deglaciation of warm-based ice between 12.4 and 12.3 ka and below 770 m asl. The scatter of exposure ages below 770 m asl can only be explained as differential "exposure inheritance" for erratics and erosion for bedrock samples. The only sample providing evidence for a burial history is UBE13 which yielded a depleted ^{26}Al/^{10}Be concentration ratio. Above 770 m asl, the range of erratic and bedrock CRN ages point to either ice-free conditions during the LGM,or, more likely, cold-based ice cover resulting in the preservation of pre-LGM surfaces and erratics (Figure 4 and Table 2).

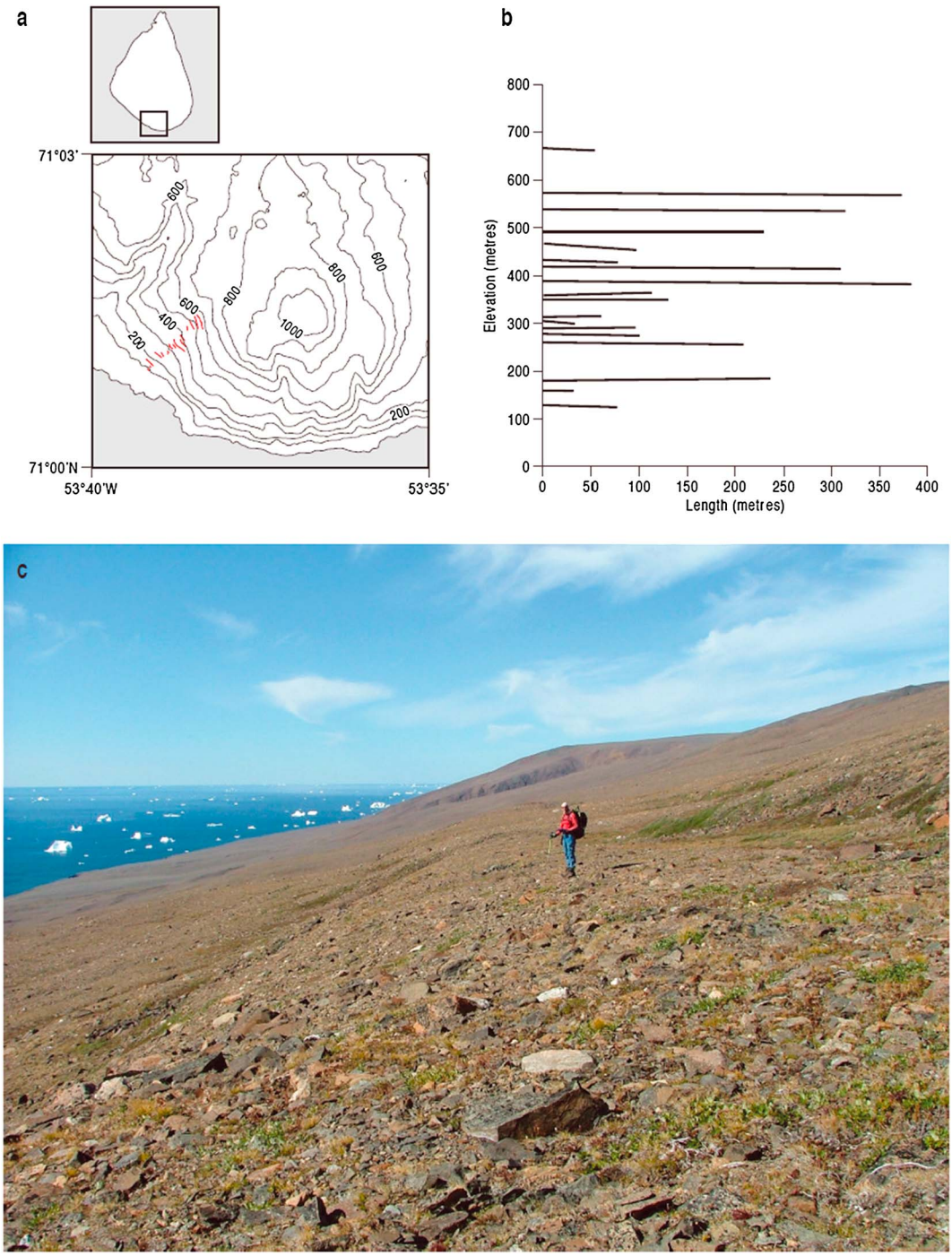

Figure 9. (a) Location of inset lateral moraine sequence on SW Ubekendt Ejland. (b) The lateral moraines reach a maximum elevation of ~670 m asl and can be traced to ~125 m asl. (c) Lateral moraine forming distinct diamictic ridge approximately 8 m high and 10 m wide.

[31] The geomorphology and chronology described above physically and temporally constrain the geometry of the UISS between Store Gletscher and Ubekendt Ejland. By assuming that at this time the GrIS was in equilibrium with climate, the geomorphology can be used to tune equilibrium profile reconstructions of the ice sheet. The key focus of this is to gain additional insight into the likely elevation of the LGM ice sheet over the current inner fjord region where there is conflicting evidence to fix the ice surface associated with the upper limit of warm-based ice operating during the LGM (e.g., inheritance on Ikerasak at 824 m asl; >100 ka surfaces and allochthonous blockfields above 750 m asl on Ivnarssup Qava; warm-based ice at >966 m asl over Drygalskis Halvø). Also presented are profiles for two other outlet glaciers north of Store Gletscher that feed into the confluence area of the Uummannaq trough and Igdlorssuit Sund, Perdlerfiup Kangerdlua and Kangerdlugssup sermia, respectively. These outlet glaciers are bounded by areally

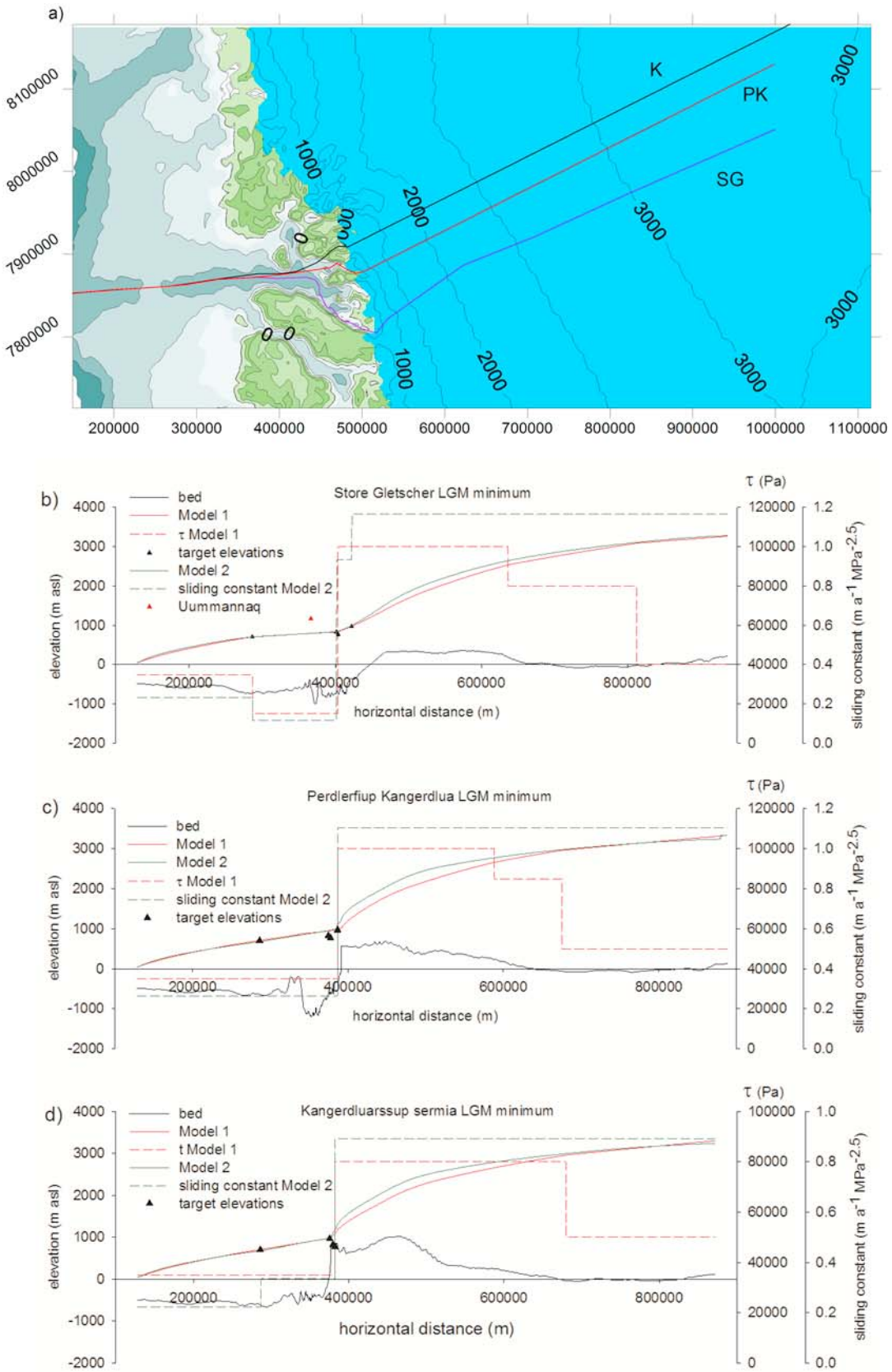

Figure 10. (a) Location of ice sheet surface profiles. SG = Store Gletscher; PK = Perdlerfiup Kangerdlua; K = Kangerdlugssup sermia. (b) Minimum LGM surface profile for Store Gletscher. (c) Minimum LGM surface profile for Perdlerfiup Kangerdlua. (d) Minimum LGM surface profile Kangerdlugssup sermia.

Table 4. Parameter Values and Errors Associated With Model Fits to Present Ice Surface

	Store Gletscher		Perdlerfiup Kangerdlua		Kangerdluarssup Sermia	
	Model 1	Model 2	Model 1	Model 2	Model 1	Model 2
RMSE (m)	30.68	39.30	19.66	10.72	9.53	9.12
Mean absolute error (m)	22.21	34.70	14.7	11.93	13.83	10.41
No. of sliding constant zones	4	1	4	4	4	4
Annual accumulation at the ice divide (m)	-	0.264	-	0.275	-	0.16

scoured terrain which is assumed to have been eroded contemporaneously with that on Drygalskis Halvø (Figure 2).

4.3.2. Matching the Present-Day Ice Sheet Surface

[32] Figure 10a shows the location of the three flow lines along which the reconstructions are undertaken. The present-day ice surface is matched using Models 1 and 2 for the three flow lines. In Model 1, the basal shear stress is varied (in zones along the flow line) until the modeled ice surface approaches the measured ice surface. In Model 2, basal shear stress, accumulation and velocity are variable. The accumulation is taken as the average across the first 50 km from the ice divide derived from *Bamber et al*. [2001, 2001]. The basal velocity is derived from the present-day surface velocity [*Bamber et al*., 2001, 2001] using the formulation of *Nye* [1952] and was averaged along the flow line. As in Model 1, the surface fit is then tuned using the basal shear stress (in 5 kPa increments) to modify A^{-m}. Table 4 presents details on the parameter values and errors achieved using each model for the three flow lines. Both models adequately reproduce the present ice sheet surface profile along each flow line. Accounting for sliding in Model 2 flattens the ice sheet profile towards the ice divide, which is well documented [e.g., *Schilling and Hollin*, 1981; *Van der Veen*, 1999], and can be clearly seen in the Store Gletscher flow line (Figure 10b). Parameter values which have been determined by fitting to the present ice sheet will be used, where possible, in the subsequent LGM reconstruction for the last 300 km of the flow line in Model 1.

4.3.3. LGM Reconstructions

[33] There are three key locations relevant to constraining the LGM elevation of the UISS: Ubekendt Ejland, Ivnarssup Qava and Ikerasak, and Drygalskis Halvø and Qarassap nunata (Figure 2). On Ubekendt Ejland in the west, the geomorphology and CRN analyses indicate an LGM ice sheet elevation of at least 700 m asl providing the first target elevation. The intermediate sites, Ivnarssup Qava and Ikerasak, provide evidence which may be interpreted as the LGM vertical limit, but the geometry of Ikerasak (streamlined and very narrow above ~750 m asl) and the presence of local, probably cold-based protective ice on Ivnarssup Qava, make any such conclusions tentative. Finally, the inner most sites Drygalskis Halvø and Qarassap nunata provide clear evidence for ice overtopping the fjord walls during the last glaciation (11.4 ka; IKE 1; Table 2 and Figure 4), while the geomorphology (very heavily abraded and streamlined) points towards warm-based ice operating at elevations significantly above the summit level of 966 m asl.

[34] Two approaches are therefore taken for the LGM reconstructions: (a) match the LGM elevation on all the key control points providing the minimum LGM ice sheet elevation such that, for example, ice was just thick enough to deposit erratics on top of Drygalskis Halvø and (b) match the LGM elevation on Ubekendt Ejland and submerge Drygalskis Halvø and Qarassap nunata beneath sufficient ice to reach the pressure melting point which in turn will determine the ice elevation over Ivnarssup Qava and Ikerasak and direct the interpretation of the dynamics there. All reconstructions are initiated from a prominent terminal moraine complex on the outer shelf [*Ó Cofaigh et al*., 2013] and extend to the current ice divide which is fixed. All flow lines are constrained by the CRN chronology on Ubekendt Ejland, but only the Store Gletscher transect is directly constrained by ground-truthed geomorphology and the remaining CRN analyses. As Perdlerfiup Kangerdlua is bounded to the north by areal scour up to ~1100 m asl and Kangerdlugssup sermia by areal scour up to 970 m asl, the elevation of Dryglaski Halvo at 966 m asl is adopted as an acceptable minimum target elevation for both. It should be noted that no corrections are made for isostatic depression or for changes in relative sea level. Ice thickness at the margin is taken as 50 m asl, the minimum level required for it to be grounded, though increasing this has little impact on the resultant ice surface after only a short distance up the flow line [*Schilling and Hollin*, 1981].

4.3.3.1. LGM Minimum Elevation

[35] Model 1: As the outer section is essentially common to all flow lines (Figures 10b–10d), they all match the 700 m asl target elevation on Ubekendt Ejland using τ = 35 kPa. Likewise, the sector between Ubekendt Ejland and the inner fjord targets for all three flow lines require τ between 15 and 35 kPa in order to keep the ice surface profile thin enough. For the Store Gletscher flow line, τ has to be ramped up from 15 kPa to 100 kPa west of Ivnarssup Qava and Ikerasak in order to even reach the top of Drygalskis Halvø (Figure 10b). Keeping τ at 35 kPa for this section gives a smooth ice surface profile for Perdlerfiup Kangerdlua to the location of the present ice margin (Figure 10c). However, the Kangerdlugssup sermia flow line requires a reduction of τ to 30 kPa (Figure 10d). Beyond the inner fjord target elevation, τ is again ramped up to between 80 and 100 kPa to the point 300 km from the present ice divide where the present day fit parameters are implemented. In all cases, this produces a reconstructed ice surface which closely mirrors the present ice surface.

[36] Model 2: Accumulation at the LGM is derived from the GISP2 ice core temperature and accumulation data set [*Cuffey and Clow*, 1997; *Alley*, 2000], averaged over the period 25–15 ka B.P. The same value of u determined for each flow line in the present-day surface fit is applied to the LGM fit. As a result, the sliding constant (fit achieved by tuning τ) required to meet the target elevation on Ubekendt Ejland differs for the three flow lines (Figures 10b–10d). For all flow lines and both models, the target on Ubekendt Ejland is met using low values of A^{-m} as would be expected due to the width of the fjord and subsequently the lack of confining

valley sides. Additionally, the bed is assumed to be composed of soft deformable sediments supporting low driving stresses and high velocities. Subsequently, the increasing trough depth along the Store Gletscher flow line, somewhat counter intuitively (i.e., the fjord narrows significantly beyond Uummannaq), requires a reduction in A^{-m} in order to just cover the summit of Ikerasak. For all flow lines, the increasing elevation of the topography from the present ice margin inland for some 100–200 km results in a very significant step in the ice surface profile if the minimum target elevation of 966 m asl is to be met.

4.3.3.2. LGM Maximum Elevation—Warm-based Ice Over the Inner Fjords

[37] The ice thickness required over Drygalskis Halvø in order for it to reach the pressure melting point is estimated using the heat conduction model of *Budd et al*. [1971], solved numerically using the spreadsheet of *Glasser and Siegert* [2002]. The same bed and surface profiles were used for the calculation as those shown in Figures 10b–10d except that the bed was elevated to 966 m asl at the appropriate location. In the spreadsheet model, the default lapse rate of $0.007°C\ m^{-1}$ was used; the geothermal heat flux was taken

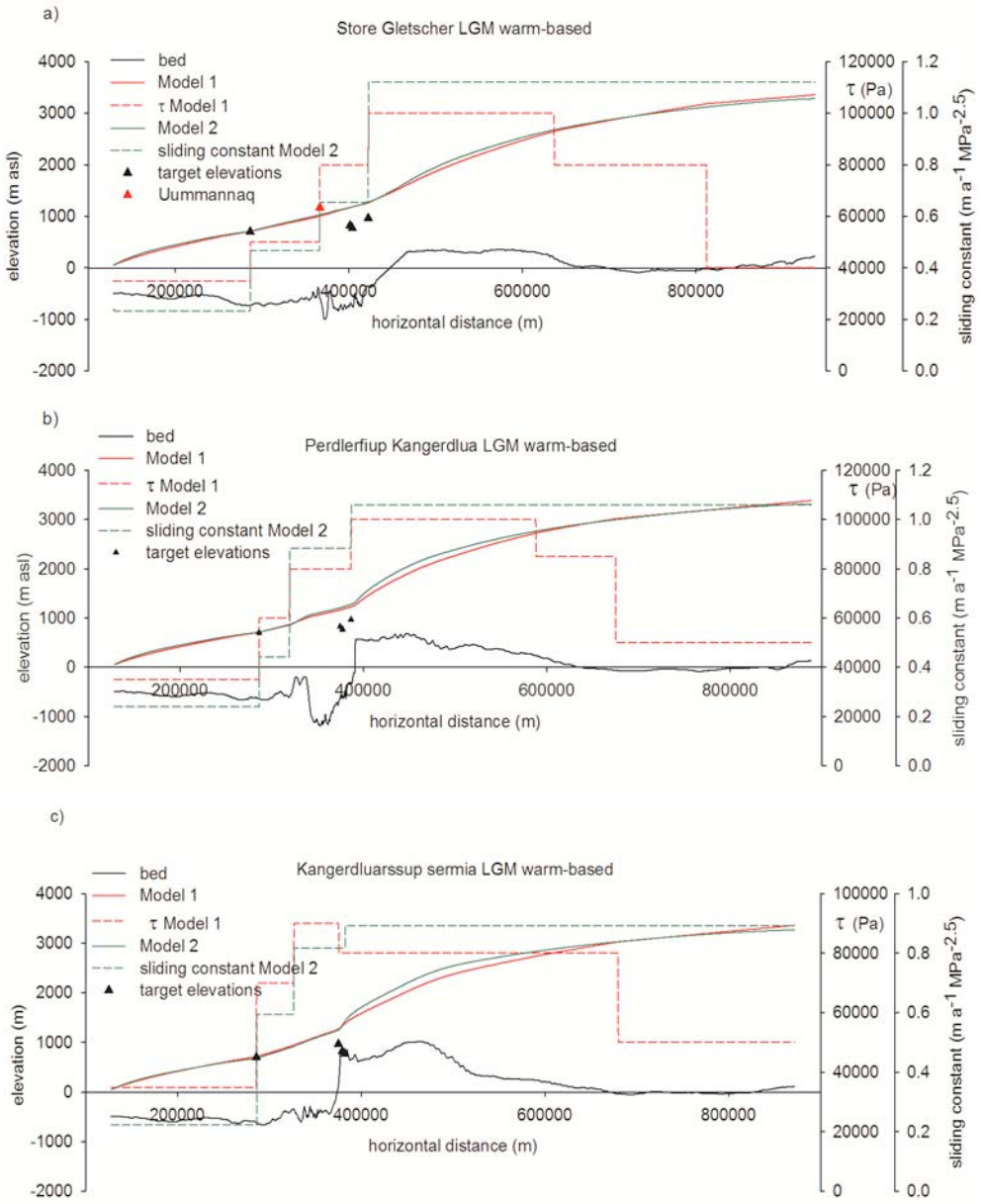

Figure 11. (a) Maximum LGM surface profile for Store Gletscher. (b) Maximum LGM surface profile for Perdlerfiup Kangerdlua. (c) Maximum LGM surface profile for Kangerdlugssup sermia.

as the continental average of 0.057 W m^{-2} [*Sclater et al*., 1980], which is probably an over estimate due to the impact of the adjacent fjord trough which focuses the heat flux into the lows [*Van der Veen*, 2007]. Accumulation at the ice divide was taken as 0.065 ma^{-1}, and the ice divide temperature was −46.8°C (averaged over the period 25–15 ka B.P.) [*Cuffey and Clow*, 1997; *Alley*, 2000]. Thus, in order for the basal ice to reach the pressure melting point, it has to be ~ 470 m thick. There are significant errors associated with this estimate, not least the impact of the topography on the geothermal heat flux into the base of the fjord and the intervening plateaux [*Van der Veen*, 2007], choice of lapse rate, and strain heating due to drawdown through the fjord heads. These could either increase or decrease the critical ice thickness, so the inner fjord target elevation for the LGM warm-based scenario is conservatively set at 1266 m asl (i.e., an ice thickness of 300 m which approximates to a 25% increase in geothermal heat flux and ice margin temperature and a 25% reduction in the lapse rate).

[38] In order to raise the ice thickness to the target elevation of 1266 m asl over Drygalskis Halvø, τ in Model 1 and A^{-m} in Model 2 have to be increased in the proximal section east of Ubekendt Ejland. In order to achieve a relatively smooth surface profile, an extra step in τ/A^{-m} (Model 1) and A^{-m} (Model 2) was introduced where the switch in bed roughness occurred (e.g., for Store Gletscher, it is associated with the trough at Uummannaq Island) and fjords narrowed significantly. As previously, the increasing elevation of the topography from the present ice margin inland for some 100–200 km results in a step in the ice surface profile (Figures 11a–11c) though this is much less dramatic than for the LGM minimum models (Figures 10b–10d).

5. Discussion

[39] At present, the principal control on outlet glacier/ice stream routing from the interior of the ice sheet to the marine terminating calving margins in the Uummannaq area is the configuration of the coastal fjords. At the LGM, the configuration of these fjords caused the convergence of multiple outlets into a confluence zone formed by Igdorlorssuit Sund and the eastern end of the Uummannaq trough (Figure 2). From this coalescent zone, the composite UISS flowed west past Ubekendt Ejland out across the shelf to the terminus. This discussion focuses on the conditions that controlled UISS onset (both spatially and temporally), LGM ice stream geometry and considers the mechanisms that controlled ice stream deglaciation from the shelf to inner coast.

5.1. Ice Stream Onset

[40] During the last glacial cycle, the role of topography would have been key in focusing ice flow. Importantly, the drawdown of ice flow into the fjord heads would have increased ice flow velocities and triggered localized ice streaming. Models 1 and 2 suggest that the ice surface steepened distally over the higher-elevation terrain up-flow from the present fjord heads and so streaming onset may well have begun as far back as the tributaries seen in present-day surface velocity maps [*Joughin et al*., 2010]. The drawdown of ice into the present-day fjord heads would have increased ice flow velocity through strain heating, and coupled with higher geothermal heat flux, most valley bottoms would have experienced increased meltwater generation at the bed. The basement bedrock has a low permeability, thus further promoting sliding [*Wellner et al*., 2001; *Hall and Glasser*, 2003] and increasing ice flux. A number of locations of heavily streamlined bedrock along the inner fjords relate to this process. For example, Drygalskis Halvø and Qarassap nunata, the lower flanks of Ikerasak (Figure 7a) and the east side of Storøen, all exhibit evidence of basal sliding and high sliding velocities in the form of streamlined bedrock terrain. Further support is provided by swath bathymetry from the confluence zone of the Ummannaq trough and Igdlorssuit Sund which indicates bed streamlining and ice flow convergence with crag and tail bedforms on the seafloor [*Ó Cofaigh et al*., 2013]. Similar streamlined terrain has been linked to thick, fast flowing ice stream activity around the margins Jakobshavn Isbrae and the Holsteinsborg Isbrae [*Roberts and Long*, 2005; *Roberts et al*., 2010].

[41] The pattern of convergent ice flow controlled by the fjord heads was the first step in UISS onset during the last glacial cycle but also critical in controlling onset conditions during successive glacial cycles is the regional geological setting, as this influenced the position of the confluence zone between Igdlorssuit Sund and the Uummannaq trough as a result of longer-term erosion. This area is underlain by a fault-bounded Cretaceous sedimentary basin which has been preferentially overdeepened on Pliocene/Pleistocene timescales, establishing a feedback of ice capture and erosion (Figure 3). Tertiary basalts to the north of Ubekendt Ejland form a topographic step (water depths are <200 m) inhibiting westward ice flow. Therefore, through multiple glacial cycles, ice from the northern sector of the UISS has been forced southward through Igdlorssuit Sund, where it has merged with ice flowing west from the southern sector of the UISS. Shortly after leaving their inner fjord mouths, both of these regional flow corridors cross from Archaen basement terrain and encounter the Cretaceous sedimentary basin where preferential erosion of the softer bedrock has led to overdeepening. Thus, Igdlorssuit Sund and the upstream areas of the Uummannaq trough form very deep troughs (>700 m), and their confluence area to the southeast of Ubekendt Ejland is the focal point for regional drawdown of the UISS (Figure 12). The long-term development of the East Greenland fjord system provides a possible analogue to the UISS. *Swift et al*. [2008] surmised that Late Cenozoic glacial erosion is largely controlled by first-order topography and geology, with selective linear erosion more prevalent in areas of Caledonian basement and less prevalent in areas of Mesozoic sedimentary rocks. Wider and larger fjords develop in downstream areas of Mesozoic strata due to their lower lithological strength which facilitates the development of fjord morphology. *Swift et al*. [2008] hypothesized that this promotes fast ice flow and the development of ice streams in manner very similar to the proposal here for the UISS.

[42] The scale at which the UISS interacts with, and evolves within, the landscape is also a critical consideration in the formation of the ice stream. In the eastern sector of the UISS onset zone, the postglacial exposure age (IKE 1; 11.4 ka; Table 2 and Figure 4) and the glacially abraded landscape (striae 284–298°) over Drygalskis Halvø and Qarassap nunata indicate that both Store and Lille Gletscher thickened sufficiently during ice advance such that ice stream surface slope

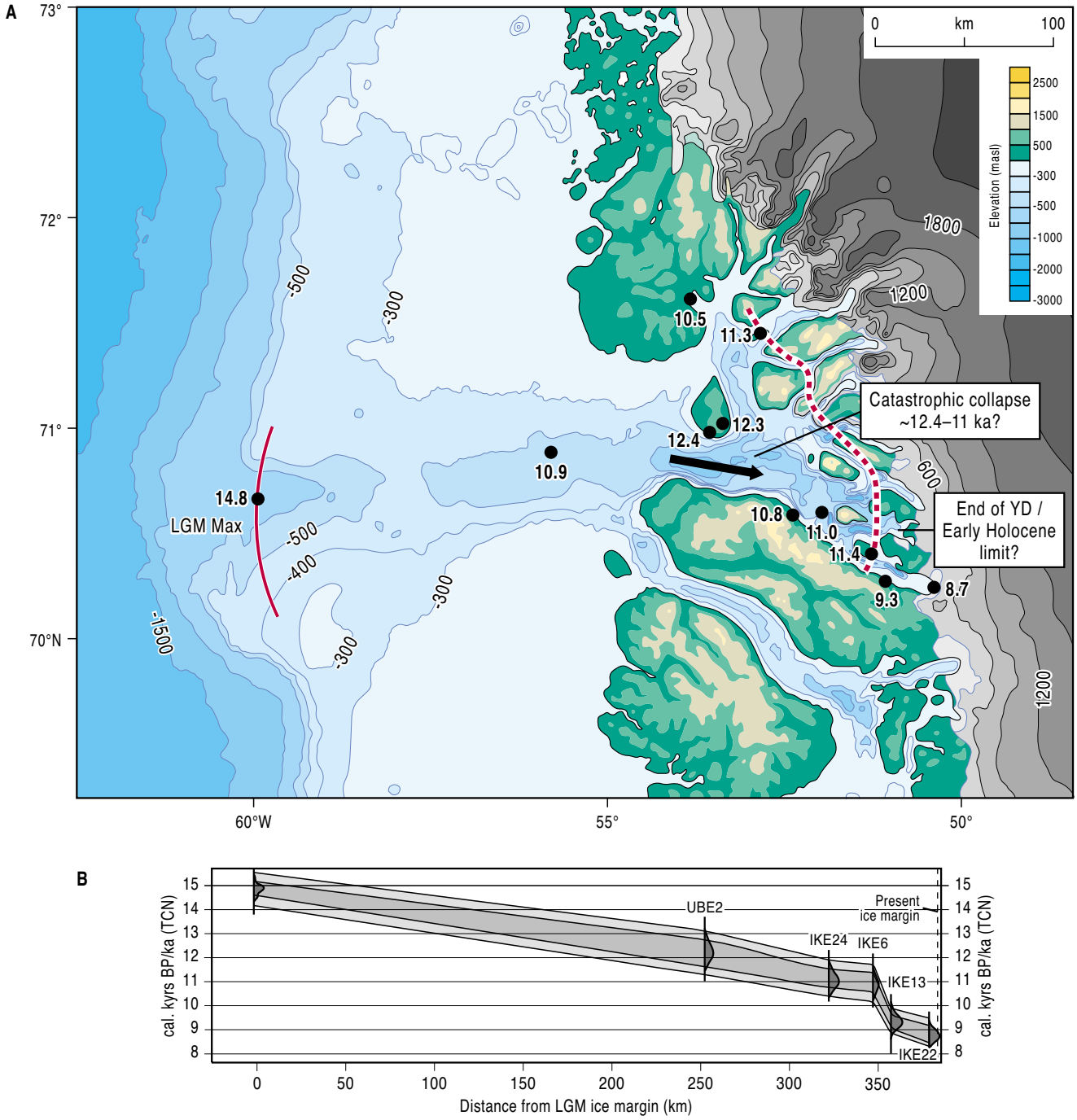

Figure 12. (a) An overview of deglacial ages along the Uummannaq trough. (b) Plot of ice margin position through time. The C^{14} age from the outer shelf (14.8 cal. kyrs B.P.) [*Ó Cofaigh et al.*, 2013] provides a minimum age for ice deglaciation. The low-elevation (<200 m asl) CRN ages between Ubekendt, Uummannaq, and Ikerasak suggest rapid deglaciation through the Uummannaq trough between ~12.4 ka and 10.8 cal. kyrs B.P. with over 100 km ice front retreat. This is followed by a period of marginal stability followed retreat eastward of the current margin between 9.3 and 8.7 ka.

guided ice flow over the topography, with ice moving westward (paralleling the Uummannaq trough). Similar diffluent behavior has been reported from Jakobshavn Isbrae, resulting in divergent flow as the ice stream submerged the topography and moved offshore (*Roberts and Long*, 2005). Thus, as ice thickened in the southern onset zone during the last glacial cycle, the fjord-head troughs became less influential in governing the flow direction of onset tributaries, while the large-scale regional topography (e.g., Nuussuuaq and Svarenhuk Peninsulas; Ubekendt Ejland; Uummannaq trough; Igdlorsuit Sund) became critical in the offshore routing of ice. In this way, the onset point for the southern sector of the UISS may have migrated westward and further offshore as ice thickened during advance.

5.2. Ice Stream Geometry

[43] At the current fjord heads around Store Gletscher and Lille Gletscher, the entire landscape up to the interfluve areas of Qarassap Nunata and Drygalskis Halvø demonstrates intense erosion beneath warm-based ice. Over interfluves areal scour and the striae directions indicate topographically unconstrained ice flow and, when combined with the modeled reconstructions (LGM warm-based), suggest an ice surface elevation in excess of ~1300 m asl (Figure 11). Based on this, the summit of Ikerasak would have been submerged beneath ~350 m of ice which would take the basal ice close to the pressure melting point. Allied to the flow-parallel orientation of the summit, it therefore seems reasonable that there is minimal evidence for scouring and TCN resetting on the summit (Figure 4). The lower surface on Ivnarssup Qava would have been submerged beneath ~400 m of ice suggesting it may have likewise been approaching the pressure melting point. However, the nature of the blockfield cover leads to the interpretation that ice cover was non-erosive with the local cold-based ice providing a protective cover and a shear margin forming above the fjord cliffs. The plateau edge moraines (Figure 6b) are likely formed during deglaciation and could potentially relate to Younger Dryas re-thickening [*Simpson et al*., 2009]. On the higher surfaces, local ice caps would have produced cold-based ice cover providing a ready explanation for the range of TCN ages, extensive blockfield cover, and weathering pits.

[44] The plateaux on Storøen are blockfield mantled above ~800 m asl suggesting that warm-based ice did not override Storøen (Figure 4). This is supported by the LGM warm-based models which show the main ice stream operating at 1000 m asl along the plateau edge (Figure 11). Therefore, a local cold-based ice cap is likely to have protected the summit from erosion. The precipitous summit of Uummannaq would have been a nunatak (1170 m asl) protruding some 150 m above the LGM ice surface as it is not wide enough to have supported a local ice cap.

[45] The southern end of Ubekendt Ejland is the critical location for demarcation of the surface of the UISS trunk zone which formed west of the Uummannaq/Igdlorsuit confluence zone at the LGM. The upper limit of ice scoured terrain is ~700 m asl with a suite of lateral moraines marking successive ice surface thinning from ~670 m down to 125 m asl (Figure 9). The landscape above 700 m asl has three surfaces covered, respectively, by till ~700–800 m asl, allochthonous blockfield ~900–1090 m asl, and autochthonous blockfield above, with erratics found up to 975 m asl. A range of exposure ages have been obtained from erratics and bedrock, but the interpretation of erratics above 700 m asl resting on blockfield and "old" till surfaces is not simple. They cannot be derived from a local cold-based ice cap activity, as they are exotic to the local basalt, micro-diorite, and granophyre bedrock, and many are well striated (Figures 8b and 8c). While they have at some point been in the basal transport zone of a warm-based ice sheet, they appear to have been deposited by cold-based ice; that is, they were deposited onto blockfield. Fieldwork in the northern fjords of the UISS has revealed evidence for warm-based ice at elevations exceeding 1400 m asl which would facilitate the emplacement of striated erratics at high elevation in the ice sheet. Additionally, compression and thickening at confluences and over topographic rises has been hypothesized to elevate erratics from basal transport onto plateau surfaces [*Sugden and Watts*, 1977]. Therefore, a conservative LGM ice stream surface elevation of 700 m asl has been chosen based on the evidence for warm-based ice and lateral moraine formation. It is likely that a cold-based summit ice field covered the highest levels of the island at LGM. Importantly, the nested lateral moraine sequence points to controlled ice stream thinning during deglaciation rather than catastrophic retreat to this pinning point following destabilization from the LGM maximum on the outer shelf. The TCN exposure data are as yet inconclusive with regards to the LGM geometry but when combined with the geomorphology provide a LGM minimum elevation. If the ice surface elevation was increased to between 900 and 1000 m asl, then the implications up-flow would be that Uummannaq was not a nunatak, with Ikerasak and Ivnarssup Qava being covered by 500–700 m of ice.

[46] From the confluence zone, the Uummannaq trough guided this large composite ice stream west for some ~200 km where it either stopped at a large terminal moraine complex sitting in the trough [*Ó Cofaigh et al*., 2013] or reached the trough mouth fan (Figure 12). The westward extension and vertical elevation of the ice stream appear to differ from previously reported LGM geometries. On Svartenhuk further to the north, *Kelly* [1985] used moraines and the lower limit of blockfields to place the LGM ice surface at ~400–450 m asl. While seemingly incompatible, these reconstructions can be rationalized if the southerly routing of ice flux from the inland ice through Igdlorsuit Sund restricted ice sheet impact over Svartenhuk, where glaciation was dominated by locally sourced ice.

5.3. UISS Deglacial Response to Local and Regional Forcing Mechanisms

[47] It has been inferred from recent cosmogenic ages, radiocarbon dates, and model output that both Holsteinborgs Isbrae and Jakobshavn Isbrae remained on the inner shelf through the Younger Dryas until the start of the Holocene (~10 ka), despite increasing air temperatures and rising sea level [*Long and Roberts*, 2003; *Roberts et al*., 2009; *Simpson et al*., 2009; *Ó Cofaigh et al*., 2013]. With respect to the UISS, a recent radiocarbon date from the outer shelf limits early deglaciation to 14.8 cal. kyrs B.P. (on benthic forams in a glaciomarine unit 5 cm above a basal till) [*Ó Cofaigh et al*., 2013]. Another recent date from the mid-shelf suggests deglaciation at ~10.9 cal. kyrs B.P. [*McCarthy*, 2011, Figure 12], but the date relates to proximal glaciomarine sedimentation and not sub-glacial conditions, and as such, it provides only a limiting constraint on deglaciation.

[48] In contrast, the two youngest deglacial CRN ages on Ubekendt suggest ice margin retreat and thinning from the shelf around 12.4 ka (UBE 14 and UBE 2; 770 m asl and 122 m asl; Figure 12 and Table 2). The lateral moraine sequence on Ubekendt Ejland (Figure 9) also suggests a sustained period of incremental top down thinning of the ice stream as it sat in the Uummannaq trough. It did not catastrophically retreat from the outer shelf eastwards of Ubekendt Ejland during early deglaciation. East of Ubekendt Ejland, the deglacial date of 10.8 cal. kyrs B.P. from Patorfik on the north coast of the Nuussuaq Peninsula plus the new, low-elevation CRN ages (coastal sites below 200 m asl) from Uummannaq and Ikerasak imply rapid

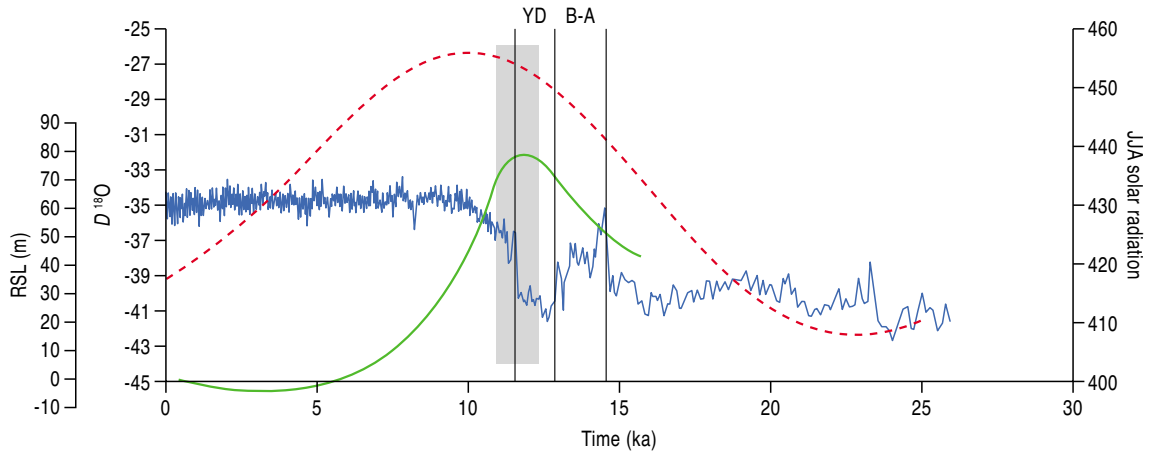

Figure 13. The GISP temperature record for the last 25 ka (blue line); the relative sea-level record (green/solid line) for Arveprinsens Ejland (85 km south of Ikerasak) [*Long et al.*, 1999; *Simpson et al.*, 2009]; seasonal mean radiation (JJA) for 70°N (red/dashed line). Note the rapid increase in air temperatures and insolation between 16.0 and 14.5 cal. kyrs B.P. in the runup to the Bølling-Allerød Interstadial. This period of warming may have driven significant surface ablation across the Uummannaq region. Rapid deglaciation (gray vertical bar denotes range of deglacial CRN ages) from Ubekendt to the fjord heads coincided to peak sea-level rise between 12.0 and 11.0 cal. kyrs B.P., and post Younger Dryas increases in air temperature and insolation.

calving through the deepest and widest parts (~800 m) of the Uummannaq trough between ~11.4 ka and 10.8 cal. kyrs B.P. (Figure 12). The deglaciation of higher-elevation topography on Drygalski Halvø and Ikerasak (IKE 1, 10, 11; 956–497 m asl) between 11.6 and 11.4 ka also infers a rapid rate of dynamic thinning of the ice stream as it calved back into its fjord heads (Figures 4 and 12). The slightly later deglacial date of 9.3 ka from Ivnarssup Qava perhaps points to Ikerasak acting as a pinning point, before the UISS underwent further Early Holocene retreat through the deep but narrow inner fjords as far as the present ice margin at Store Gletscher by 8.7 ka (Figures 4 and 12). Fjord Stade moraines mapped on the eastern side of Drygalski Halvo (*Weidick*, 1968) have been dated elsewhere in central West Greenland to between 10.0 and 7.5 cal. kyrs B.P. [*Long et al.*, 2006; *Briner et al.*, 2010] and would provide a broad corroboration with this deglacial chronology; however, field investigations in 2009 failed to identify the Fjord Stade moraines previously reported.

[49] Overall, this pattern of deglaciation is broadly similar to other West Greenland LGM ice stream systems. The lateral moraines on Ubekendt Ejland could relate to an early phase of UISS thinning in response to increasing mean summer (JJA) insolation followed by increased air temperatures between 16 and 14.5 cal. kyrs B.P. in the run up to the Bølling Interstadial (Figure 13) [cf. *Roberts et al.*, 2009; *Van de Berg et al.*, 2011]. It is possible that the ice stream remained on the shelf during the Younger Dryas [cf. *Rinterknecht et al.*, 2009; *Simpson et al.*, 2009; *Roberts et al.*, 2010; *Ó Cofaigh et al.*, 2013], and the moraines that overtop the inner fjord walls at ~750 m asl on Ivnarssup Qava may relate to Younger Dryas re-thickening, but the evidence from Ubekendt contradicts that hypothesis as retreat and thinning was ongoing at 12.4–12.3 ka.

[50] Rapid retreat post-12.4 ka is evident from the new CRN ages and older C^{14} record from Patorfik, Uummannaq and particularly Ikerasak, which all suggest ice stream retreat into the inner fjords between ~11.4 ka and 10.8 cal. kyrs B.P. (Figures 4 and 12), though it should be noted that all the low-elevation CRN and radiocarbon ages from the mid-shelf to Ikerasak overlap within a 2 sigma age range. This early retreat of the UISS compared to both Jakobshavn and Holsteinborg Isbraes [*Roberts et al.*, 2010] may have been a response to widening of the trough east of Ubekendt Ejland as well as increased water depth (Figure 13) [cf. *Pfeffer*, 2007; *Briner et al.*, 2009; *Schoof*, 2007; *Jamieson et al.*, 2012]; however, this period also coincides with peak sea-level rise, increasing insolation, and rapidly increasing air temperatures post the Younger Dryas (Figure 13), all of which can increase surface ablation and grounding line instabilities leading to accelerated calving [*Nick et al.*, 2010]. The UISS is unlikely to have been driven from the shelf by increased ocean temperatures [cf. *Knutz et al.*, 2011] as recent work by *McCarthy* [2011] constrains the arrival of the warm West Greenland Current into this region to 8.4 cal. kyrs B.P., much too long into the Holocene to influence initial shelf deglaciation. The southern sector of the UISS may have briefly stabilized around narrow topographic pinning points such as Ikerasak before deglaciating fully into its fjord heads between 9.3 and 8.7 ka as Holocene air and ocean temperatures rose, although localized standstills analogous to those reported from Jakobshavn Isbrae may have occurred during this time in response to abrupt cooling events [*Young et al.*, 2011].

6. Conclusions

[51] The UISS was a large composite ice stream that drained the Greenland ice sheet during the last glacial cycle. The formation of the UISS was triggered through a convergent network of regional fjords which formed as a result of long-term selective linear erosion. These guided multiple small ice streams and outlet glaciers to the coast, where flow

converged into a geologically controlled, overdeepened confluence zone triggering ice stream onset. The UISS then moved offshore along the Uummannaq trough towards the shelf edge break. This process has occurred multiple times, and hence, it is hypothesized that the UISS is a product of concomitant erosional feedback operating throughout the Quaternary. Glacially scoured landscapes up to 1000 m asl in fjord-head areas were produced by warm-based ice moving offshore during the last glacial cycle. As ice thickened, it became diffluent above 1000 m asl, and as onset the zone developed, local fjords oriented oblique to ice flow became less influential in controlling ice flow pathways, perhaps allowing onset zone migration to the west. Model output of the UISS surface suggests that warm-based ice may have operated up to a minimum of 1266 m asl, but as ice flowed westwards, the elevation of warm-based erosion dropped to ~700 m asl as the UISS trunk zone developed further offshore.

[52] High-elevation plateaux exhibit both allochthonous and autochthonous blockfield, suggesting that warm-based ice did, at some point in the past, produce till and erratics up to ~1200 m asl in the landscape, but CRN ages and weathering pits suggest that this was pre-LGM, with only cold-based local ice caps operating during the last glacial cycle. This assumption is supported by modeled ice surface projections which suggest that even if warm-based ice was operating at ~1266 m in inner fjord areas, it would not have been sufficient to trigger warm-based erosion of high plateau surfaces. This is consistent with the idea that more efficient fjord networks reduce the thickness, volume, and extent of ice during successive glaciations.

[53] Between 14.8 cal. kyrs B.P. and 12.4 ka, the outer/middle shelf and Ubekendt Ejland became ice free though further dating control is required to confirm this and to test if the UISS remained on the mid-shelf throughout the Younger Dryas. Following this, the UISS underwent a rapid collapse with over 100 km of eastward retreat to Uummannaq and Ikerasak by ~11.4 ka - 10.8 cal. kyrs B.P. Retreat may have accelerated east of Ubekendt Ejland because of fjord widening and bathymetric overdeepening, but rising sea level, increasing insolation, and air temperatures were also contributing factors. The retreat of the UISS to the inner coast occurred prior to significant ocean warming in this region which was not prevalent on the Uummannaq shelf until ~8.4 cal. kyrs B.P. The ice stream margin was temporarily stabilized by inner fjord pinning points, before Early Holocene retreat continued between 9.3 and 8.7 ka in response to both increasing air and ocean temperatures. Determining and understanding the processes that control the dynamic behavior of large cross-shelf ice stream systems such as the UISS during periods of pronounced climatic variability remains vital if we are to improve predictions of future ice sheet stability.

[54] **Acknowledgments.** This work was supported by the Department of Geography (Durham University), the Department of Geography (University of Aberdeen), the Carnegie Trust for Scottish Universities, and NERC CIAF Grant 9063/0409. Our special thanks go to Matthew Wright, Birte Ørum, and Arne Neumann who supported logistical operations; NERC CIAF staff for the preparation of cosmogenic samples; and Sheng Xu at the SUERC AMS facility. The Design and Imaging Unit, Department of Geography, Durham University, is also thanked for the production of numerous figures. We also thank reviewers Darrel Swift, Nicolaj Larsen, and Vincent Rinterknecht for very helpful and useful comments on the paper.

References

Andresen, C. S., et al. (2012), Rapid response of Helheim Glacier in Greenland to climate variability over the past century, *Nat. Geosci.*, *5*, 37–41

Alley, R. B. (2000), The Younger Dryas cold interval as viewed from central Greenland, *Quat. Sci. Rev.*, *19*, 213–226.

Balco, G., J. O. Stone, N. A., Lifton, and T. J. Dunai (2008), A complete and easily accessible means of calculating surface exposure ages or erosion rates from ^{10}Be and ^{26}Al measurements, *Quat. Geochron.*, *3*, 174–195.

Balco, G., J. Briner, R. C. Finkel, J. A. Rayburn, J. C. Ridge, and J. M. Schaefer (2009), Regional beryllium-10 production rate calibration for northeastern North America, *Quat. Geochron.*, *4*, 93–107.

Ballantyne, C. K. (1997), Periglacial trimlines in the Scottish Highlands, *Quat. Int.*, *38/39*, 119–136.

Ballantyne, C. K., C. Schnabel, and S. Xu (2009), Exposure dating and reinterpretation of coarse debris accumulations (rock glaciers) in the Cairngorm Mountains, Scotland., *J. Quat. Sci.*, *24*, 19–31.

Bamber, J. L., S. Ekholm, and W. B. Krabill (2001a), A new, high-resolution digital elevation model of Greenland fully validated with airborne laser altimeter data, *J. Geophys. Res.*, *106*, 6733–6745.

Bamber, J. L., R. J. Hardy, and I. Joughin (2000), An analysis of balance velocities over the Greenland ice sheet and comparison with synthetic aperture radar interferometry, *J. Glac.*, *46*, 67–74.

Bamber, J. L., R. L. Layberry, and S. P. Gogenini (2001b), A new ice thickness and bedrock elevation data set for Greenland: Part I, *J. Geophys. Res.*, *106*, 33, 773–780.

Benn, D. I., and N. R. J. Hulton (2010), An ExcelTM spreadsheet program for reconstructing the surface profile of former mountain glaciers and ice caps, *Comp. Geosci.*, *36*, 605–610.

Bennike, O. (2000), Palaeoecological studies of Holocene lake sediments from West Greenland, *Palaeogeogr., Palaeoclimatol., Palaeoecol.*, *155*, 285–304.

Bennike, O., K. B. Hansen, K. L. Knudsen, D. N. Penney, and K. L. Rasmussen (1994), Quaternary marine stratigraphy and geochronology in central West Greenland, *Boreas*, *23*, 194–215.

Bennike, O., and S. Björck (2002), Chronology of the last recession of the Greenland Ice Sheet, *J. Quat. Sci.*, *17*, 211–219.

Bierman, P. R., K. A. Marsella, C. Patterson, P. T. Davis, and M. Caffee (1999), Mid-Pleistocene cosmogenic minimum-age limits for pre-Wisconsin glacial surfaces in southwestern Minnesota and southern Baffin Island: A multiple nuclide approach, *Geomorph.*, *27*, 25–39.

Bjørk, A. A., K. H. Kjær, N. K. Korsgaard, S. A. Khan, K. K. Kjeldsen, C. S. Andresen, J. E. Box, N. K. Larsen, and S. Funder (2012), An aerial view of 80 years of climate-related glacier fluctuations in southeast Greenland, *Nat. Geosci.*, *5*, 427–432.

Block, A. E., and R. E. Bell (2011), Geophysical evidence for soft bed sliding at Jakobshavn Isbrae, West Greenland, *The Cryosphere*, *5*, 339–366.

Briner, J. P., G. H. Miller, P. T. Davis, and R. C. Finkel (2006), Cosmogenic radionuclides from fiord landscapes support differential erosion by overriding ice sheets, *Geol. Soc. Am. Bull.*, *118*, 406–420.

Briner, J. P., A. C. Bini, and R. S. Anderson (2009), Rapid early Holocene retreat of a Laurentide outlet glacier through an Arctic fjord. *Nat. Geosci.*, doi:10.1038/ngeo556.

Briner, J. P., H. A. M. Stewart, N. E. Young, W. Philipps, and S. Losee (2010), Using proglacial-threshold lakes to constrain fluctuations of the Jakobshavn Isbrae ice margin, western Greenland, during the Holocene, *Quat. Sci. Rev.*, *29*, 3861–3874.

Briner, J. P., N. S. Young, E. M. Brent, M. Goehring, and J. M. Schaefer (2012), Constraining Holocene ^{10}Be production rates in Greenland, *J. Quat Sci.*, *27*(1), 2–6.

Box, J. E., D. E. Bromwich, B. A. Veenhuis, L.-S. Bai, J. E. Stroeve, J. C. Roger, K. Steffen, T. Haran, and H. H. Wang (2006), Greenland Ice Sheet surface mass balance variability (1988–2004) from Calibrated Polar MM5 Output, *J. Clim.*, *19*, 2783–2800

Brett, C. P., and E. F. K. Zarudzki (1979), Project Westmar: A shallow marine geophysical survey on West Greenland continental shelf, *Rapp.*, *87*, Grønlands Geologiske Undersøgelse, Copenhagen.

Budd, W. F., D. Jenssen, and U. Radok (1971), Derived physical characteristics of the Antarctic ice sheet, ANARE Interim Reports, Series A. Glaciology. Publication No 120.

Chalmers, J. A., C. Pulvertaft, C. Marcussen, and A. K. Pedersen (1999), New insight into the structure of the Nuussuaq Basin, central West Greenland. *Mar. Pet. Geol.*, *16*, 197–224.

Cuffey, K. M., and G. D. Clow (1997), Temperature, accumulation and ice sheet elevation in central Greenland through the last deglacial transition, *J. Geophys. Res.*, *102*(C12), 26383–396.

Dahl, R. (1966), Blockfields, weathering pits and tor-like forms in the Narvik Mountains, Nordland, Norway, *Geogr. Ann.*, *48A*, 55–85.

Di Nicola, L., C. Schnabel, K. M. Wilcken, and K. Gméling (2009), Determination of chlorine concentrations in whole rock: Comparison between prompt-gamma activation and isotope-dilution AMS analysis, *Quat. Geochron.*, *4*, 501–507.

Dunne, J., D. Elmore, and P. Muzikar (1999), Scaling factors for the rate of production of cosmogenic nuclides for geometric shielding and attenuation at depth on sloped surfaces, *Geomorph.*, *27*, 3–11.

Echelmeyer, K. A., and W. D. Harrison (1990), Jakobshavn Isbrae, West Greenland: Seasonal variations in velocity—or lack thereof, *J. Glac.*, *36*, 82–88.

Echelmeyer, K. A., W. D. Harrison, C. Larsen, and J. E. Mitchell (1994), The role of the margins in the dynamics of an active ice stream, *J. Glac.*, *40*, 527–538.

Evans, J., C. O´Cofaigh, J. A. Dowdeswell, and P. Wadhams (2009), Marine geophysical evidence for former expansion and flow of the Greenland Ice Sheet across the northeast Greenland continental shelf, *J. Quat. Sci.*, *24*, 279–293.

Funder, S., and L. Hansen (1996), The Greenland ice sheet—A model for its culmination and decay during the after the Last Glacial Maximum, *Bull. Geol. Soc. Den.*, *42*, 137–152.

Glasser, N., and C. Warren (1990), Medium-scale landforms of glacial erosion in southern Greenland: process and form, *Geog. Ann.*, *72*, 211–215.

Glasser, N. F., and M. J. Siegert (2002), Calculating basal temperatures in ice sheets: An EXCEL spreadsheet method, *Earth Surf. Proc. Land*, *27*, 673–680.

Gordon, J. E. (1981), Ice scoured topography and its relationships to bedrock structure and ice movement in parts of northern Scotland and West Greenland, *Geog. Ann.*, *63*, 55–65.

Håkansson, L., J. Briner, H. Alexandersson, A. Aldahand, and G. Possnerte (2007), ^{10}Be ages from central east Greenland constrain the extent of the Greenland ice sheet during the Last Glacial Maximum, *Quat. Sci. Rev.*, *26*, 2316–2321.

Hall, A., and N. Glasser (2003), Reconstructing the basal thermal regime of an ice stream in a landscape of selective linear erosion: Glen Avon, Cairngorm Mountains, Scotland, *Boreas*, *32*, 191–208.

Holland, D. M., R. H. Thomas, B. deYoung, M. H. Ribergaard, and B. Lyberth (2008), Acceleration of Jakobshavn Isbrae triggered by warm subsurface ocean waters, *Nat. Geosci.*, doi:10.1038.

Howat, I. M., I. Joughin, S. Tulaczyk, and S. Gogineni (2005), Rapid retreat and acceleration of Helheim Glacier, East Greenland, *Geophy. Res. Lett.*, *32*, L22502, doi:10.1029/2005GL024737.

Hughes, A. L. C., E. Rainsley, T. Murray, C. Fogwill, C. Schnabel, and S. Xu (2012), Rapid response of Helheim Glacier, southeast Greenland, to early Holocene climate warming, *Geology*, *40*, 427–430.

Iken, A., K. A. Echelmeyer, W. D. Harrison, and M. Funk (1993), Mechanisms of fast flow in Jakobshavn Isbrae, West Greenland: Part 1. Measurements of temperature and water-level in deep boreholes, *J. Glac.*, *39*, 15–25.

Jamieson, S. J. R., N. J. R. Hulton, and M. Hagdorn (2008), Modelling landscape evolution under ice sheets, *Geomorph.*, *97*, 91–108.

Jamieson, S. J. R., A. Vieli, S. J. Livingstone, C. Ó. Cofaigh, C. Stokes, C.-D. Hillenbrand, and J. Dowdeswell (2012), Ice-stream stability on a reverse bed slope, *Nat. Geosci.*, doi:10.1038/ngeo1600.

Jennings, A. E., M. Hald, and M. Smith (2006), Freshwater forcing from the Greenland Ice Sheet during the Younger Dryas: Evidence from southeastern Greenland shelf cores, *Quat. Sci. Rev.*, *25*, 282–298.

Joughin, I. (2006), Climate change-Greenland rumbles louder as glaciers accelerate, *Science*, *311*, 1719–1720.

Joughin, I., and R. Alley (2011), Stability of the West Antarctic ice sheet in a warming world, *Nat. Geosci.*, *4*, 506–513

Joughin, I., B. E. Smith, I. M. Howat, T. Scambos, and T. Moon (2010), Greenland flow variability from ice-sheet-wide velocity mapping, *J. Glac.*, *56*, 415–430.

Kelly, M. (1985), A review of the Quaternary geology of western Greenland, in Quaternary Environments in Eastern Canadian Arctic, Baffin Bay and Western Greenland, edited by J. T. Andrews, pp. 461–501, Allen and Unwin, Boston.

Kessler, M. A., R. S. Anderson, and J. P. Briner (2008), Fjord insertion into continental margins driven by topographic steering of ice, *Nat. Geosci.*, *1*, 365–369.

Knutz, P. C., M.-A. Sicre, H. Ebbesen, S. Christiansen, and A. Kuipers (2011), Deglacial retreat of the southern GreenlandIce Sheet linked with Irminger Current warm water transport, *Paleoceanography*, *26*, PA3204, doi:10.1029/2010PA002053.

Layberry, R. L., and J. L. Bamber (2000), A new ice thickness and bed data set for the Greenland ice sheet: 2. Relationship between dynamics and basal topography, *J. Geophys. Res.*, *106*, 33,781–788.

Larsen, N. K., K. H. Kjær, J. Olsen, S. Funder, K. K. Kjeldsen, and N. Nørgaard-Pedersen (2011), Restricted impact of Holocene climate variations on the southern Greenland Ice Sheet, *Quat. Sci. Rev.*, *30*, 3171–3180.

Long, A. J., and D. H. Roberts (2003), Late Weichselian deglacial history of Disko Bugt, West Greenland, and the dynamics of Jakobshavns Isbrae ice stream, *Boreas*, *32*, 208–226.

Long, A. J., D. H. Roberts, and M. R. Wright (1999), Isolation basin stratigraphy and Holocene relative sea-level change on Arveprinsen Eijland, Disko Bugt, West Greenland, *J. Quat. Sci.*, *14*, 323–345.

Long, A. J., D. H. Roberts, and S. Dawson (2006), Early Holocene history of the West Greenland Ice Sheet and the GH-8.2 event, *Quat Sci. Rev.*, *25*, 904–922.

Luckman, A., T. Murray, R. de Lange, and E. Hanna (2006), Rapid and synchronous ice dynamic changes in East Greenland, *Geophys. Res. Lett.*, *33*, L03503.

Lykke-Andersen, H. (1998), Neogene-Quaternary depositional history of the East Greenland shelf in the vicinity of leg 152 shelf sites, in Proceedings of the Ocean Drilling Program, Scientific Results, edited by A. D. Saunders, H. C. Larsen, and S. W. Wise Jr., 152, pp. 29–38, College Station, TX.

Maden, C., P. A. F. Anastasi, D. Dougans, S. P. H. T. Freeman, R. Kitchen, G. Klody, C. Schnabel, M. Sundquist, K. Vanner, and S. Xu (2007), SUERC AMS ion detection, *Nuc. Inst. Meth.*, *B259*, 131–139.

Marsella, K. A., P. R. Bierman, P. Tompson-Davis, and M. W. Caffee (2000), Cosmogenic ^{10}Be and ^{26}Al ages for the Last Glacial Maximum, eastern Baffin Island, Arctic Canada, *GSA Bull.*, *112*, 1296–1312.

McCarthy, D. (2011), Late Quaternary ice-ocean interactions in central West Greenland, PhD Thesis, Dept. of Geog., Durham University, UK.

Nesje, A., and S. O. Dahl (1990), Autochthonous block fields in southern Norway: Implications for the geometry, thickness, and isostatic loading of the Late Weichselian Scandinavian ice sheet, *J. Quat. Sci.*, *5*, 25–234.

Nick, F. M., A. Vieli, I. M. Howat, and I. Joughin (2009), Large-scale changes in Greenland outlet glacier dynamics triggered at the terminus, *Nat. Geosci.*, 110–114.

Nick, F. M., C. J. Van Der Veen, A. Vieli, and D. I. Benn (2010), A physically based calving model applied to marine outlet glaciers and implications for the glacier dynamics, *J. Glac.*, *56*(199), 781–794.

Nishiizumi, K., E. L. Winterer, C. P. Kohl, J. Klein, R. Middleton, D. Lal, and J. R. Arnold (1989), Cosmic ray production rates of ^{10}Be and ^{26}Al in quartz from glacially polished rocks, *J. Geophys. Res.*, *94*, 17907–17915.

Nye, J. (1952), The mechanics of glacier flow, *J. Glac.*, *2*, 82–93.

Ó Cofaigh, C., J. A. Dowdeswell, J. Evans, N. H. Kenyon, J. Taylor, J. Mienert, and M. Wilken (2004), Timing and significance of glacially influenced mass-wasting in the submarine channels of the Greenland Basin, *Mar. Geol.*, *2207*, 39–54.

Ó Cofaigh, C., et al. (2013), An extensive and dynamic ice sheet on the West Greenland shelf during the last glacial cycle, *Geology*, *41*, 219–222.

Phillips, W. M., A. M. Hall, C. K. Ballantyne, S. Binnie, P. W. Kubik, and S. Freeman (2008), Extent of the last ice sheet in northern Scotland tested with cosmogenic ^{10}Be exposure ages, *J. Quat. Sci.*, *23*, 101–107.

Pfeffer, W. T. (2007), A simple mechanism for irreversible tidewater glacier retreat, *J. Geophys. Res.*, doi:190 10.1029/2006JF000590.303.

Rea, B. R. W. B., M. M. R. Whalley, and J. E. Gordon (1996), Blockfields: Old or new? Evidence and implications from some plateaus in northern Norway, *Geomorph.*, *15*, 109–121.

Rignot, E., and P. Kanagaratnam (2006), Changes in the velocity structure of the Greenland Ice Sheet, *Science*, *311*, 986–990.

Rinterknecht, V. R., Y. Gorokhovich, J. M. Schaefer, and M. Caffee (2009), Preliminary ^{10}Be chronology for the last deglaciation of the western margin of the Greenland Ice Sheet, *J. Quat. Sci.*, *24*, 270–278.

Roberts, D. H., A. J. Long, B. Davies, and C. Schnabel (2010), Ice stream influence on west Greenland Ice Sheet dynamics during the Last Glacial Maximum, *J. Quat. Sci.*, *25*, 850–864.

Roberts, D. H., A. J. Long, C. Schnabel, M. Simpson, and B. Davies (2009), Ice sheet extent and deglacial history of the central western sector of the Greenland Ice sheet, *Quat. Sci. Rev.*, *28*, 2760–2773.

Roberts, D. H., A. J. Long, C. Schnabel, M. Simpson, and S. Freeman (2008), The deglacial history of the southeast sector of the Greenland ice sheet during the Last Glacial Maximum, *Quat. Sci. Rev.*, *27*, 1505–1516.

Roberts, D. H., and A. J. Long (2005), Streamlined bedrock terrain and fast ice flow, Jakobshavns Isbrae, West Greenland: Implications for ice stream and ice sheet dynamics, *Boreas*, *34*, 25–42.

Schilling, D. H., and J. T. Hollin (1981), Numerical reconstructions of valley glaciers and small ice caps, in The Last Great Ice Sheets, edited by G. H. Denton, and T. J. Hughes, pp. 207–220, Wiley, New York.

Schimmelpfennig, I., L. Benedetti, R. Finkel, R. Pik, P. H. Blard, D. Bourlés, P. Burnard, and A. Williams (2009), Sources of in-situ 36Cl in basaltic rocks. Implications for calibration of production rates, *Quat. Geochronol.*, *4*, 441–461.

Schoof, C. (2007), Ice sheet grounding line dynamics: Steady states, stability, and hysteresis, *J. Geophys. Res.*, *112*, F03S28.

Sclater, J. G., C. Jaupart, and D. Galson (1980), The heat flow through oceanic and continental crust and the heat loss of the Earth, *Rev. Geophys. Space Phys.*, *18*, 269–311.

Simonarson, L. A. (1981), Upper Pleistocene and Holocene marine deposits and faunas on the north coast of Nugssuaq, West Greenland, *Bull. Grønlands Geol. Unders.*, *40*, 1–107.

Simpson, M. R., G. Milne, P. Huybrechts, and A. J. Long (2009), Calibrating a glaciological model of the Greenland ice sheet from the last glacial maximum to present-day using field observations of relative sea level and ice extent, *Quat. Sci. Rev.*, *28*, 1631–1657.

Solheim, A., J. I. Faleide, E. S. Andersen, A. Elverhoi, C. F. Forsberg, K. Vanneste, G. Uenzelmann-Neben, and J. E. T. Channell (1998), Late Cenozoic seismic stratigraphy and glacial geological development of the East Greenland and Svalbard-Barents Sea continental margins, *Quat. Sci. Rev.*, *17*, 155–184.

Straneo, F., G. S. Hamilton, D. A. Sutherland, L. A. Stearns, F. Davidson, M. O. Hammill, G. B. Stenson, and A. Rosing-Asvid (2010), Rapid circulation of warm subtropical waters in a major glacial fjord in East Greenland, *Nat. Geosci.*, *3*, 182–186.

Stone, J. O. (2000), Air pressure and cosmogenic isotope production., *J. Geophys. Res.*, *105*, 753–759.

Sugden, D. E., N. Glasser, and C. M. Clapperton (1992), Evolution of large roches moutonneés, *Geog. Ann.*, *74*, 253–264.

Sugden, D. E. (1974), Landscapes of glacial erosion in Greenland and their relationship to ice, topographic and bedrock conditions, Institute of British Geographers Special Publication, 7, 177–195.

Sugden, D. E., and S. H. Watts (1977), Tors, felsenmeer, and glaciationsin northern Cumberland Peninsula, Baffin Isand, *Can. J. Earth Sci.*, *14*, 2817–2823.

Swift, D. A., C. Persano, F. M. Stuart, K. Gallagher, and A. Whitham (2008), A reassessment of the role of ice sheet glaciation in the long-term evolution of the East Greenland fjord region, *Geomorphology*, *94*, 109–125.

Truffer M., and K. A. Echelmeyer (2003), Of Isbrae and ice streams, *Ann. Glac.*, *36*, 66–72.

van de Berg, W. J., M. van den Broeke, E. Janneke, E. V. Meijgaard, and F. Kaspar (2011), Significant contribution of insolation to Eemian melting of the Greenland ice sheet, *Nat. Geosci.*, *4*, 679–683.

Van der Veen, C. J. (1999), Fundamentals of Glacier Dynamics, Balkema, Rotterdam.

Van der Veen, C. J. (2007), Fracture propagation as means of rapidly transferring surface meltwater to the base of glaciers, *Geophys. Res. Lett.*, *34*, L01501, doi:10.1029/2006GL028385.

van Tatenhove, F. G., A. Fabre, R. Greve, and P. Huybrechts (1996), Modelled ice-sheet margins of three Greenland ice-sheet models compared with a geological record from ice-marginal deposits in central West Greenland, *Ann. Glac.*, *23*, 52–58.

Velicogna, I., and J. Wahr (2006), Acceleration of Greenland ice mass loss in spring 2004, *Nature*, *443*, 329–331.

Vieli, A., and F. M. Nick (2011), Understanding and modelling rapid dynamic changes of tidewater outlet glaciers: Issues and implications, *Surv. Geophys.*, *32*, 437–458.

Vincent, P. J., P. Wilson, T. C. Lord, C. Schnabel, and K. M. Wilcken (2010), Cosmogenic isotope (^{36}Cl) surface exposure dating of the Norber erratics, Yorkshire Dales: Further constraints on the timing of the LGM deglaciation in Britain, *Proc. Geol. Assoc.*, *121*, 24–31.

Weidick, A. (1968), Observations on some Holocene glacier fluctuations in West Greenland, *Meddel. om Grönl.*, *165*, 1–202.

Weidick, A., and O. Bennike (2007), Quaternary glaciation history and glaciology of Jakobshavn Isbræ and the Disko Bugt region, West Greenland: A review, *Geol. Surv. Den. and Green. Bull.*, No 14.

Wellner, J. S., A. L. Lowe, S. S. Shipp, and J. B. Anderson (2001), Distribution of glacial geomorphic features on the Antarctic continental shelf and correlation with substrate: Implications for ice sheet behaviour, *J. Glac.*, *47*, 397–411.

Wilson, P., M. J. Bentley, C. Schnabel, R. Clark, and S. Xu (2008), Stone run (block stream) formation in the Falkland Islands over several cold stages, deduced from cosmogenic isotope (^{10}Be and ^{26}Al) surface exposure dating, *J. Quat. Sci.*, *23*, 461–473.

Young, N. E., J. P. Briner, H. A. M. Stewart, Y. Axford, B. Csatho, D. Rood, and R. C. Finkel (2011) Response of Jakobshavn Isbræ, Greenland, to Holocene climate, *Geology*, *39*, 131–134.

Zwally, H. J., W. Abdalati, T. Herring, K. Larson, J. Saba, and K. Steffen (2002), Surface melt-induced acceleration of Greenland ice-sheet flow, *Science*, *297*, 218–222